INFORMATION TO USERS

This manuscript has been reproduced from the microfilm master. UMI films the text directly from the original or copy submitted. Thus, some thesis and dissertation copies are in typewriter face, while others may be from any type of computer printer.

The quality of this reproduction is dependent upon the quality of the copy submitted. Broken or indistinct print, colored or poor quality illustrations and photographs, print bleedthrough, substandard margins, and improper alignment can adversely affect reproduction.

In the unlikely event that the author did not send UMI a complete manuscript and there are missing pages, these will be noted. Also, if unauthorized copyright material had to be removed, a note will indicate the deletion.

Oversize materials (e.g., maps, drawings, charts) are reproduced by sectioning the original, beginning at the upper left-hand corner and continuing from left to right in equal sections with small overlaps.

Photographs included in the original manuscript have been reproduced xerographically in this copy. Higher quality 6" x 9" black and white photographic prints are available for any photographs or illustrations appearing in this copy for an additional charge. Contact UMI directly to order.

Bell & Howell Information and Learning
300 North Zeeb Road, Ann Arbor, MI 48106-1346 USA
800-521-0600

Optical Sensing of Thermoplastics Solidification in an Injection Moulding Machine

by

Edgar C. Ramírez Domínguez

Department of Chemical Engineering
McGill University, Montréal
August 1998

A thesis submitted to the Faculty of Graduate Studies and Research in partial fulfillment of the requirements for the degree of Master of Engineering

Abstract

An optical technique for monitoring the solidification of thermoplastics in an injection moulding machine was implemented. The technique uses a He-Ne laser that illuminates the mould cavity, and a photomultiplier to measure the intensity of reflected light during the moulding cycle. Data from the sensor allows tracking the injection moulding cycle development. The measured light intensity is mainly influenced by refraction and reflection phenomena at the melt-solid interfaces during solidification. Reflection occurs primarily from the opposite mould wall but the reflection intensity is a complex composite of reflective scattering and refraction from crystallites, the mould wall and as many as six interfaces. The scattering caused by the opposite mould wall roughness also affects the light intensity. Plots of reflection intensity during the injection moulding cycle obtained for the three materials tested show similar patterns. Polystyrene, polypropylene and high-density polyethylene resins were used. The higher scattering power of semi-crystalline polyethylene and polypropylene reduces the reflection intensity values compared to the polystyrene plots. Further experimental and analytical work is required to use this technique for process control purposes.

Résumé

Une technique optique pour étudier la solidification des thermoplastiques dans une machine de moulage par injection a été développée. Cette technique utilise un laser qui illumine la cavité du moule, et un photomultiplicateur pour mesurer l'intensité de la lumière réfléchie pendant le cycle de moulage. Les données du capteur permettent de suivre le développement du cycle du moulage par injection. L'intensité de lumière mesurée est principalement influencée par les phénomènes de réflexion et de réfraction à l'interface liquide-solide pendant la solidification. La réflexion intervient majoritairement à la paroi opposée du moule. L'intensité de la réflexion est une combinaison complexe de la diffraction provoquée par multiple réflexions, et de la réfraction des crystallites, de la paroi du moule, et de jusqu'à six interfaces. La diffraction qui est causée par le rugosité de la paroi opposée du moule influence également l'intensité lumineuse. Pour les trois matériaux testés, polystyrene, polypropylene, et polyethylene haute densité, les tracés de l'intensité lumineuse pendant le cycle du moulage par injection montrent des résultats similaires. La plus grande capacité de diffraction des résines semi-crystallines, i.d. le polypropylene et le polyethylene, réduit leur intensité de réflexion comparée à celle du polystyrene. Il est nécessaire d'approfondir cette technique de manière expérimentale et analytique pour pouvoir l'utiliser à des fins de contrôle du procédé de fabrication.

Acknowledgements

I wish to express my deep gratitude to my research supervisors, Prof. W. Ian Patterson and Prof. Musa R. Kamal. Their valuable advice, support, and critical review of this work were fundamental for its development and completion.

I thank Mr. Lou Cusmich, Mr. Alain Gagnon and the personnel of the Machine Shop for their professional response to the diverse work requirements that arose during this project.

The diverse assistance and inputs from my fellow graduate students of the Chemical Engineering department are greatly appreciated, particularly from Mr. Oscar Rodríguez, Dr. Mehdi Rafizadeh, Dr. Hamid Garmabi, Ms. Julie Lin, and Mr. Lei Wang. Special thanks to Mr. Ludovic Capt for translating the abstract into French, and Mr. José Ramón Hernández for taking care of details of this thesis's submission.

I am grateful for the financial support received as a Government of Canada Award, and an assistantship from McGill University. The support from the Instituto Tecnológico de Zacatepec is also appreciated. Thanks to Dow Chemical Canada Inc., Montell North America Inc., and Nova Chemicals Ltd. for supplying the resins used in the experimental work.

Finally, I would like to express my deepest gratitude to my family, very specially my mother, my brother and sisters, for their love, support and encouragement. The opportune support from my cousin Francisco Fernando Contreras is greatly appreciated. Most of all I am indebted to my partner of joys and trouble, work and fun. With love, to my wife Betty.

Para tí.

Table of Contents

List of Figures

List of Tables

Nomenclature

Cp	specific heat
G	shear modulus
i	angle of incident light
I	light intensity
k	thermal conductivity
k_a	adiabatic bulk modulus
L	path traversed by a light beam
M	molar mass of a polymer structural unit
n	refractive index
NEP	noise equivalent power
p	pressure
Pn	nozzle pressure
r	angle of refracted light
R	reflection power
R_{LL}	molar refraction
T	temperature
Tc	temperature of cooling water
u_l	ultrasound velocity in a compressible liquid
u_s	ultrasound velocity in an elastic solid
v	specific volume
κ	coefficient of extinction
λ	light wavelength
ρ	density

Chapter 1

Introduction

Injection moulding is one of the most widely used processes in the modern plastics industry. Recent estimates show that approximately 25 % of the total production of plastics goods in industrialized countries are produced using the injection moulding process [1,2]. Its acceptance is due, among other factors, to the versatility, high production rates, and low cost per unit that characterize it. Normal injection moulding machines produce parts in the range 200-2000 g, with cycles of 3-10 s. More specialized injection moulding machines are known to produce small parts of fractions of a gram, while others deliver products weighting around 20 kg.

The injection moulding process is integrated by a cyclic sequence of operations as follows. Initially, the temperature of a polymer resin is raised beyond its melting point, so it reaches conditions where it will flow under pressure. The polymer melt is injected into a mould, where it is allowed to solidify under high pressure. Finally, the mould is opened and the solid part is ejected to prepare for the next cycle.

1.1 Motivation

The development of techniques and devices to monitor and control the operation of the injection moulding process is a very important issue in the plastics industry. Research at McGill University and other polymer groups in the world has focused on the instrumentation and control of injection moulding machines. Significant contributions have been reported in the monitoring and control of pressure, temperature, and part weight [3,4,5,6,7]. One of the fundamental reasons for the interest in monitoring injection moulding is that without proper control, the operation of injection moulding machines

(IMM) may vary substantially and produce a large number of unacceptable, out-of-specifications parts.

The control of IMMs is currently not directly related to end product characteristics. In fact, the properties of injection moulded products are strongly affected by the rate of solidification of the polymer melt inside the mould. The reason for this correlation is that the final morphology and state of the solid product are determined during solidification. Unfortunately, there is no accepted direct way to monitor the solidification rate of the melt inside the mould. This is largely due to the lack of dependable, non-intrusive methods that do not interfere with the solidification or blemish the product. The harsh conditions of high temperature, pressure, and shear rate inside the mould impose restrictions on the operation and utility of many types of sensors.

Several techniques for characterization of polymeric materials may provide useful information concerning the characteristics of the solidification of melt inside the mould cavity of IMMs. In particular, techniques based on the use of electromagnetic radiation are interesting. These techniques satisfy the requirement of being non-intrusive, so potentially they are applicable to the injection moulding solidification monitoring problem. A few cases of the application of electromagnetic radiation for on-line monitoring of polymer processing have appeared in the literature. Preliminary reported results appear promising; they are discussed in Chapter 2. It is still to be verified if such techniques demonstrate the sensitivity and simplicity of operation sought in an appropriate solidification sensor.

1.2 Objectives

The two primary objectives of this research were:

1. To design and implement a technique for monitoring solidification of polymer melt inside the mould cavity of an injection moulding machine.

2. To test and analyze the performance of the selected technique.

A secondary objective was to determine the technique feasibility for process control purposes.

1.3 Thesis Organization

This thesis is organized according to the following structure. Relevant technical background to this work is presented in Chapter 2, as well as the theoretical foundations for the technique used. The design and construction of the sensor is described in Chapter 3. The tests, analysis and results obtained from the experimental work are presented in Chapter 4, along with a discussion of the performance of the sensor. Chapter 5 contains the conclusions reached from this work.

Chapter 2

Technical Background

A brief description of the injection moulding process is the first topic presented in this chapter. Next, reports of relevant research on the instrumentation and control of the injection moulding (IM) process are analyzed. A discussion about the extent to which the final properties of injection moulded products can be controlled is also presented. Finally, an introduction to the principles that govern the operation of an optical sensor for monitoring melt solidification is given.

2.1 The Injection Moulding Process

The injection moulding process is a cyclical sequence of mechanical operations used to transform solid polymer materials supplied in the form of pellets into plastics products shaped according to product specifications. Apart from the specific shape, other characteristics that are also sought in final injection moulded products include dimensional stability, mechanical and optical properties. Usually products must meet specifications regarding tensile and impact strength, shrinkage and warpage. Specifications related to optical properties usually include color, clarity, haze, and gloss [1].

The most common injection moulding machine (IMM) in the industry is the reciprocating screw type. Its main components may be grouped into three units: the hydraulic system, the clamping unit, and the injection unit. The IMM at McGill University is of the reciprocating screw type, and the process description here is restricted to such a machine. Figure 2.1 shows a sketch of a reciprocating screw IMM.

The injection moulding unit includes a hopper, an extruder screw and barrel. The barrel is heated, usually by electric heaters. The clamping unit consists of a fixed platen and a

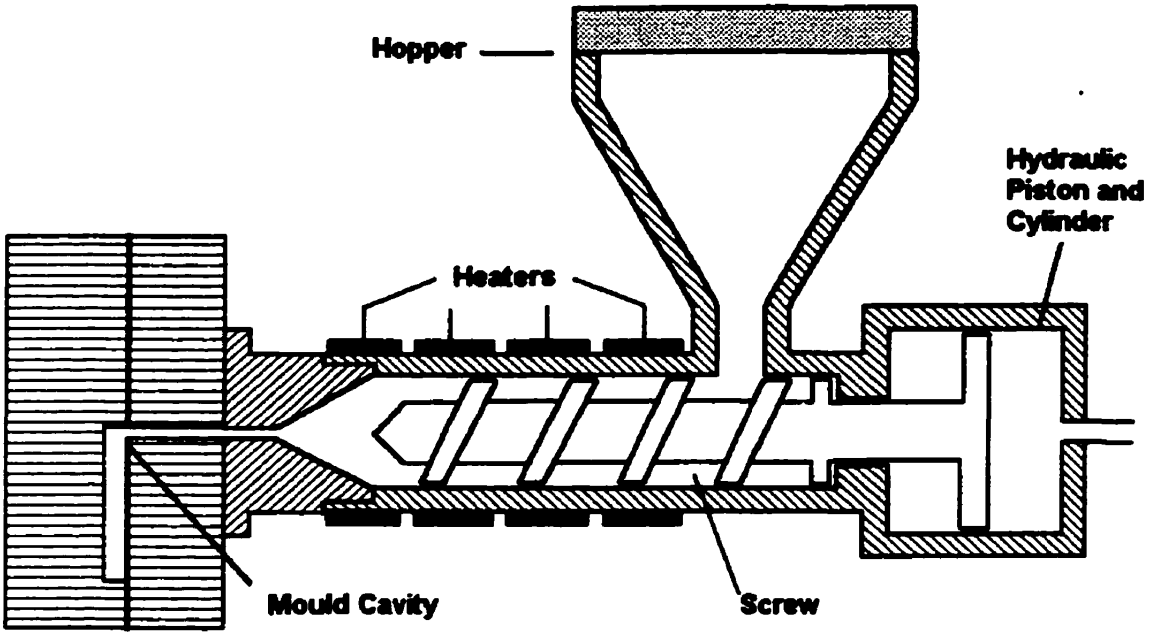

Figure 2.1 Sketch of a reciprocating injection moulding machine

movable platen, which form a mould cavity when closed and are in contact with each other. The mould is cooled by external services, usually water. The necessary piping, pump, and motor form the hydraulic unit, which supplies hydraulic power to the clamping and injection moulding units.

During the start-up of the injection moulding (IM) process, the barrel and screw are empty and polymer pellets are supplied from the hopper to the extruder barrel, where they are melted by the heaters and the shear heating (viscous dissipation) due to the screw rotation. The same rotational movement conveys melt to the front of the barrel, between the screw tip and the nozzle. Once there is melt at the operational temperature in the front of the barrel, the process may be operated in a cycle consisting of the following phases.

2.1.1 Injection Moulding Phases

In the initial phase, called "filling", the hydraulic unit supplies power for the clamping unit to close from its initially open position. At the beginning of filling, the screw ceases

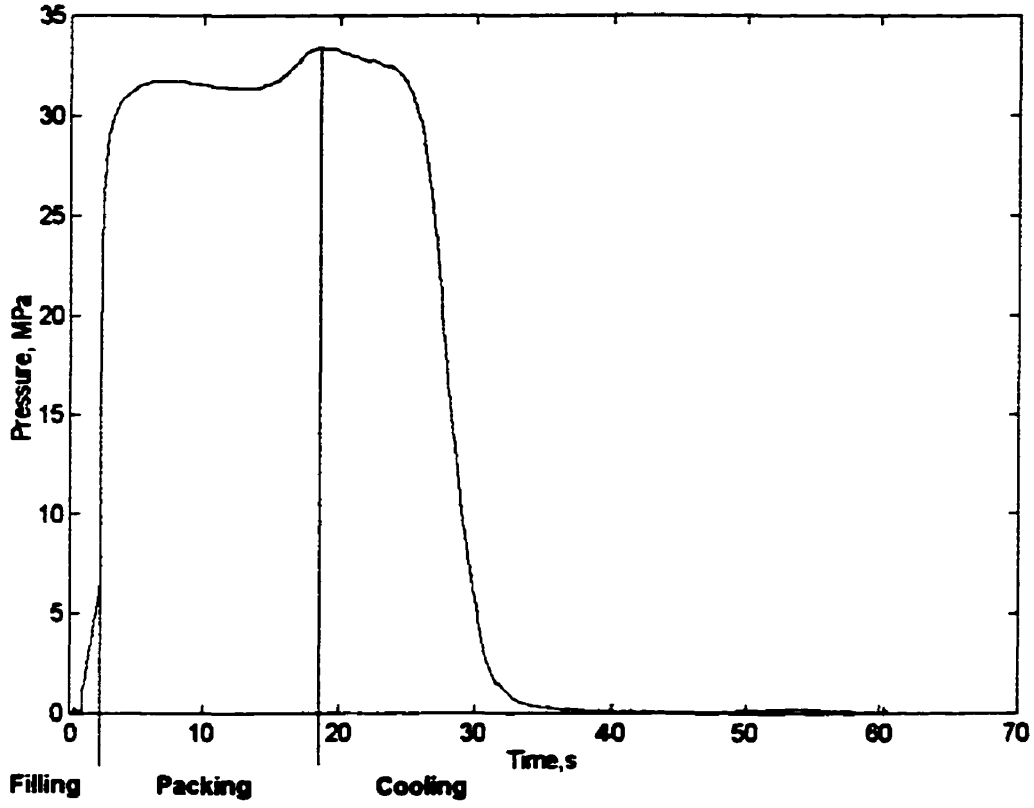

Figure 2.2 Typical profile of cavity pressure during an injection moulding cycle for HDPE

to rotate, and the hydraulic motor supplies power to advance the screw so that melt is injected into the mould cavity completely filling it. Figure 2.2 shows the cavity pressure-time profile for injection moulding of high-density polyethylene (HDPE). The "filling" phase is characterized by the gradual increase of cavity pressure, until the complete filling of the mould, when the pressure sharply increases.

The "packing" phase follows after filling. During this phase, high pressure is maintained inside the cavity by keeping pressure applied on the screw. The purpose is to inject additional melt to compensate for shrinkage of the moulded part during solidification. Hence, during this phase the profile shows no significant decrease in the cavity pressure.

The "cooling" phase starts when the polymer melt at the cavity gate solidifies, and the part inside the mould becomes isolated from the injection unit. Cooling of the moulded specimen proceeds for the time necessary according to process specifications. In Figure 2.2 it can be appreciated that the cavity pressure decreases from the level held during packing to zero. During the cooling phase, the screw moves back and rotates to convey more melt to the front of the barrel. At the end of this phase the clamping unit opens, and the moulded part is ejected. The next injection moulding cycle starts from this point.

To obtain parts of consistently the same characteristics, the injection moulding process requires a precise coordination of the functional units of IMMs, i.e. the injection moulding unit, the clamping unit, and the hydraulic system. Process specifications depend on final product requirements and on rheological and thermophysical properties of materials. Process monitoring and control are extremely important to obtain precise interactions among the units of IMMs.

2.1.2 Characteristics of Thermoplastics for Injection Moulding

Thermoplastics are materials that, in their finished state, contain as an essential ingredient a synthetic polymer of high molecular weight, are either a flexible or rigid solid, and at some point during its processing can be shaped by flow and converted to solid by cooling of the melt [1]. The characteristics of a plastic derive from the very long molecular chain, and the ability of its segments to rotate around their bonds. Polymer chains that do not have profuse or irregular branching permit partial crystallization. The large length and relative size difference of polymer chains do not allow the occurrence of perfectly crystalline polymers. Other polymers whose chains contain large branches or side chains cannot accommodate crystalline structures upon solidification, and remain amorphous. Additionally, because many entanglements occur among the polymer chains, orientation effects develop when the material flows.

Semi-crystalline polymer melts that solidify under different thermodynamic conditions may develop different degrees of crystallinity. Both amorphous and semi-crystalline polymers may reach different orientation degrees depending on processing conditions. The degree of crystallinity and orientation of polymers largely influence the physical properties of the final products, as described below [1,8].

- Crystallinity gives a more compact structure, so density increases with crystallinity.
- Stiffness is higher for crystalline materials compared to an amorphous plastic of the same molecular weight and of similar chemical structure. This occurs because crystalline structures hinder the rotation of segments, thereby reducing the material flexibility.
- The tensile strength increases with increasing crystallization. This follows from the extra force per unit volume needed to break the closer bonds of a compact crystalline structure than that needed for an amorphous material. Orientation of polymer chains further increases tensile strength of solid polymers along the orientation axis.
- Crystalline structures tend to rapidly propagate impact energy along the faces of the crystals where they break. Hence, increasing values of crystallinity reduce the impact strength. On the other hand, orientation increases the impact strength along the orientation axis, sometimes more than 100 % for materials such as high-impact polystyrene [1].
- Increasing crystallinity decreases the specific volume, thus increasing shrinkage. This is caused by the difference between the volume occupied by the amorphous melt and the smaller volume occupied by ordered crystalline structures.
- Concerning optical properties, higher crystallinity usually will cause less transparency and more haze. Yet it has been reported in [8] that for nylon and polypropylene the transparency increases for higher crystallinity. Optical properties are influenced by other factors as well (e.g. the presence of pigments and fillers in the polymer, the surface finishing), so often there is no simple correlation between crystallinity and the optical properties. Orientation causes different refractive index values for the material along the orientation axis, compared to the value along the normal to the orientation axis. This is perceived as birefringence.

2.2 Instrumentation and Control of Injection Moulding Machines

A great deal of work has been focused on the instrumentation of injection moulding machines. Several research groups have produced significant work related to the control of injection moulding machines [3,5,6,9]. Currently, many of the operational parameters of IMM can be monitored. The ultimate purpose of such work is to control the process, so that injection moulded products consistently meet all specifications.

It is useful to distinguish between process variables and machine variables associated with the operation of IMMs. The machine variables are those associated with the direct operation of the machine or its components. Usually, machine variables can be measured and controlled directly. Typical machine variables include screw rotational speed, hydraulic pressure, barrel temperature, and cooling water temperature. The process condition is described by the process variables. They are correlated to the machine variables. The control and manipulation of machine variables is aimed to influence the values of process variables. Examples of the process variables are cavity pressure, melt temperature, melt viscosity, and rate of solidification.

Important final characteristics of injection moulded products are controlled by the values of the process variables. In particular, the rate of solidification of the polymer melt inside the mould cavity determines properties such as residual stresses and the degree of crystallinity of semi-crystalline polymer products. Properties such as optical clarity, tensile strength, warpage and total shrinkage of moulded specimens are determined in part by the amount of residual stresses and degree of crystallinity. Thus, the rate of solidification inside the mould cavity is a primary factor in the injection moulding process.

Monitoring and control of the rate of solidification is difficult due to restrictions imposed by the injection moulding operating conditions. It is necessary to employ non-intrusive means, so that no interference with the shape or appearance of the moulded specimen is

caused. The mould cavity is under high pressure, moderate temperature conditions that the sensor must withstand. Real time response is required for control purposes.

A review of techniques applied to monitoring of polymer processing revealed that the most feasible options available to monitor the solidification rate may be sensors based on the use of ultrasound or electro-magnetic radiation. Optical and ultrasound techniques are promising because of their non-intrusive nature. Both the intensity of light transmitted through materials and the velocity of ultrasound are influenced by the density of the medium. Techniques based on X-rays scattering or polarized light encounter difficulties to install detection and focusing devices in the platens and mould. Sensors that require substantial modifications to the mould are undesirable, as the stress deformation resistance of the platens must not be considerably affected.

2.2.1. Optical Techniques for Monitoring Melt Solidification

Optical techniques have been successfully used in the characterization of polymer crystallization and blend morphology. The research of Stein and coworkers [10] has led to the development of a light scattering technique for characterizing spherulite formation in crystallizing melts. The technique is based on the analysis of the images produced on a photographic film by a beam of polarized light that travels through a thin sample. However, this technique analyzes only very thin polymer specimens, so it is not applicable for on-line monitoring of thick specimen crystallization in injection moulding machines.

Several approaches have been followed towards the development of an effective solidification sensor. Bur et al [11] tested two optical techniques, reporting varying degrees of success. One of their techniques is based on the measurement of fluorescence intensity from doped polymer inside the mould cavity. An optical window installed on the movable plate allowed excitation of the fluorescent dye by means of a light source. The fluorescence intensity measurements could be correlated to the evolution of the injection

moulding cycle, as the activities of the dyes used depend on temperature and pressure. They claimed that the fluorescence intensity pattern during the injection cycle leads to a correlation with the stages of the cycle. The authors identified the injection and packing phases in relation to the time of occurrence of changes in the intensity pattern. However, several drawbacks arise with the use of this technique. The use of fluorescent dyes may be inconvenient for certain industrial applications. Also, large scattering effects of pigmented and filled resins may affect or invalidate this technique.

The same authors tested an optical approach for monitoring solidification in the mould cavity based on the analysis of light scattering [12,13]. During the injection moulding cycle, the mould cavity was illuminated with a laser beam sent through an optical window installed on the movable wall of the mould. The light beam traveled the thickness of the melt inside the cavity, and was reflected from the opposite fixed wall of the mould. The intensity of the reflected light was measured throughout the cycle. It was found that the stages of the cycle could also be identified and tracked by analyzing the reflected light intensity. The variation of the intensity obeys several optical laws, which were not analyzed in detail by the authors.

A technique based on the use of optical coherence tomography for evaluation of semi-transparent media was reported [14]. A light source provides illumination for a sample, through one arm of an interferometer. A reference mirror receives part of the source light through another arm of the interferometer. Then the two reflected beams are recombined and detected in a photodetector. The resulting pattern provides a reflectivity profile of the sample. On the basis of preliminary experiments, it is claimed that the images of the microstructure show higher resolution than ultrasound results. This technique has not been applied to an actual injection moulding process. Also, it is not clear how far below the surface the measurement can be performed.

Recently, a light-scattering photometer for in-line studies of morphology during polymer extrusion was reported by Li et al [15]. The instrument features two optical windows mounted on opposing sides of the slit die of an extruder. The windows are the entry and

exit ports for incident light. A He-Ne laser is used as the light source, and a video camera records the intensity changes. The same arrangement of optical windows is used to allow the use of an optical microscope that is also used to visualize morphological details of the extruded melt. The authors utilized the instrument to analyze the dispersion of low volume fractions of polyethylene and polystyrene. Overall, this instrument appears to be convenient for on-line morphology and flow characterization in polymer processing machines. Yet its use in the mould cavity of an IMM may be very difficult due to the restrictions found to install delicate focusing devices and/or sophisticated sensors on the platens of IMMs.

2.2.2. Ultrasound Techniques for Monitoring Melt Solidification

Ultrasound technology has been applied to monitoring polymer-processing conditions [18,19], after being initially used for characterization of polymers and polymer blends [16, 17].

Gendron et al [16] reported the convenience of using techniques based on the measurement of the attenuation and velocity of ultrasound for monitoring the dispersion of minor phases of polypropylene/polyethylene and polypropylene/polystyrene blends. Experiments were run over the entire range of compositions. A correlation of ultrasound attenuation with the degree of mixing was detected. It was concluded that different degrees of attenuation are caused by blends with coarse dispersion of the minor phase, compared to well-dispersed blends that behave like single-phase polymers. The sensitivity of ultrasound to differentiate between single-phase or multiphase polymers suggests that it may also be suitable for the melt-solidification monitoring problem, in the case of semi-crystalline materials. However, an analysis of the bulk modulus difference range for which ultrasound attenuation may distinguish between single-phase and multiphase melts would be required.

Piché et al [18] examined the ultrasound velocity in confined samples of polypropylene melt that were allowed to undergo solidification. Their results show that ultrasound velocity under these conditions is controlled by the values of viscosity associated with small molecular mobility. From a second experiment, the authors found that the ultrasound velocity in a polymer melt flowing in an extruder can be analyzed by assuming a multilayer structure. Anomalous ultrasound attenuation near the walls of the extruder led the authors to assume the existence of an interface layer between the walls and the core. The authors recognized that more work is needed to understand the dynamics of interfacial mobility and shear stress, and how they affect ultrasound velocity.

An ultrasound sensor was installed in the mould of an IMM by Thomas et al [19]. The filling and packing stages of the cycle were monitored. The authors reported that the velocity of ultrasound varied as the melt went through solidification inside the mould. According to the dependence of sound velocity on density and bulk modulus of the material, a characteristic change in the value of velocity will be noticed when the material undergoes phase change. The ultrasound velocity of a wave propagating in an elastic solid is given by [19]:

$$u_s = \sqrt{\frac{k_a + \frac{4}{3}G}{\rho}} \qquad 2\text{-}2$$

and the ultrasound velocity for a wave propagating in a compressible liquid is given by:

$$u_l = \sqrt{\frac{k_a}{\rho}} \qquad 2\text{-}1$$

where $\mathbf{u}$ is the velocity

$\mathbf{k_a}$ is the adiabatic bulk modulus

$\mathbf{G}$ is the shear modulus

ρ is the density

2.2.3 Selection of a Technique for Monitoring Melt Solidification

Several limitations are imposed on the monitoring technique by the nature of the injection moulding process. The technique must be non-intrusive as in the case of optical and ultrasound based techniques. An additional factor is the difficulty of installing a sensor at the cavity wall. The fixed platen of the McGill IMM already has many cavity transducers and thermocouples that leave little room for the installation of other sensors. Both platens have cooling channels that limit the available area for installation of other sensors as well. Relatively small sensors are required to fit in the limited available space on the platens. This is also desirable in industrial practice.

The feasibility of ultrasound technology for the monitoring of melt solidification is yet to be demonstrated by means of further experimentation. In particular, the attenuation of ultrasound caused by polymer flow is not well understood [18]. This effect may occur during the early packing stage of injection moulding as additional melt is injected into the mould.

The construction of an optical sensor based on the reflection of visible light as proposed by Bur and Thomas [12] appeared to be a promising approach. In addition to meeting the process restrictions, its response is almost entirely controlled by the solidification phenomena. An analysis of the optical effects related to the operation of such a sensor follows.

2.3 Fundamentals of a Reflection Based Technique for Monitoring Melt Solidification

The reflection technique proposed by Bur and Thomas [12] tracks and analyzes changes in the intensity of a light beam as it travels through the solidifying melt inside the mould cavity, according to the sketch presented in Figure 2.3. When a beam of light is propagated in a material medium, its velocity is less than its velocity in vacuum and its

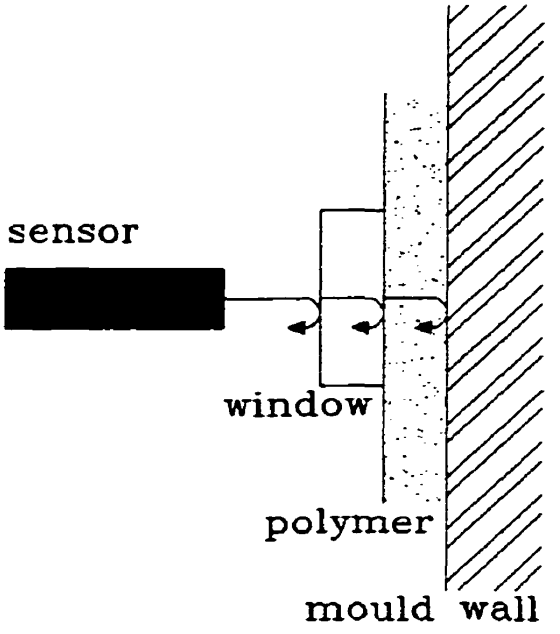

Figure 2.3 Configuration of the optical sensor proposed in [12]

intensity gradually decreases as it progresses through the medium. The reduction in the intensity is partly due to the fact that some light is scattered and part of it is absorbed [20]. In the case of semi-crystalline melts undergoing partial crystallization, the scattering of light is caused by crystalline structures that are large compared with the light wavelength. Therefore, the scattering consists of a mixture of diffraction and diffuse reflection and refraction.

The refraction phenomenon determines the extent of deviation of a light beam when it passes from one medium to another having a different refractive index at an angle other than 90° to the interface, as illustrated in Figure 2.4. The basic law of optical refraction was formulated by Snell [20].

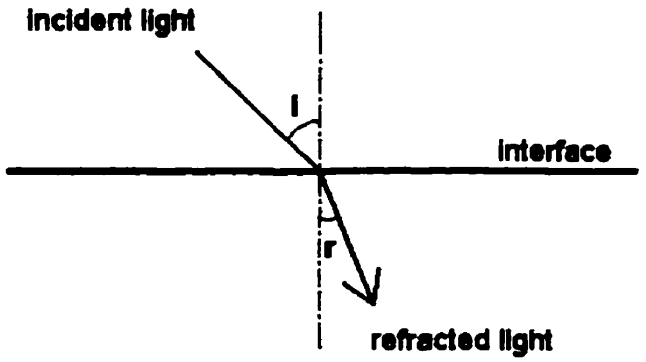

Figure 2.4 Refraction of light

$$n \sin i = n' \sin r \qquad \text{2-3}$$

where n, n' are the indices of refraction of the materials

i, r are the angles of incident and refracted light.

In the present case, refraction occurs when the light beam enters the polymer in the cavity due to the practical impossibility of producing an incident beam perfectly normal to the specimen surface. Further refraction is expected to occur crossing the boundaries between solid and liquid phase of the polymer as the light traverses the cavity and is reflected from the opposite wall. See Figure 4.11 (page 68).

The reflection at a boundary plane between two non-absorbing media is a function of the two refractive indices of the media examined. The reflection coefficient or reflecting power R is the ratio of the reflected to the incident intensity and, for a normal incidence, it may be obtained from Fresnel's equation [20]:

$$R = \frac{(n_2 - n_1)^2}{(n_2 + n_1)^2} \qquad \text{2-4}$$

where n_2, n_1 are the refractive indices of the two media.

Some reflection of the light beam is expected at the boundaries between window and polymer. The main reflection is expected to be from the opposite cavity wall of the mould, back to the polymer specimen. The reflection at the opposite wall of the mould may be obtained from Beer's equation. For an absorbing medium R is expressed as:

$$R = \frac{(n_2 - n_1)^2 + n_2^2\kappa^2}{(n_2 + n_1)^2 + n_2^2\kappa^2} \qquad \text{2-5}$$

where κ is the coefficient of extinction of the absorbing material.

A beam of light with wavelength λ propagating through a medium over a path L suffers a loss of intensity due to absorption characterized by Lambert's relationship:

$$I = I_0 \exp\left(-\frac{4\pi n\kappa L}{\lambda}\right) \qquad \text{2-6}$$

where I, I_0 are the final and initial light intensities.

The variations of the refractive index and the extinction coefficient as a function of temperature and pressure are very relevant for the operation of the reflection sensor. The most significant changes in these parameters are expected just when the melt undergoes phase transition upon solidification.

Van Krevelen [21] cited the work of Gladstone and Dale [22], which indicated that the ratio $(n-1)/\rho$ is a characteristic constant of the substance considered. The term *molar refraction*, R_{LL}, was used to denote the relationship between this constant and the molar mass; this relationship was found to have additive properties. Its units are volume/mol. Several expressions for the molar refraction are reported in [21]. One of the generally accepted relationships is the Lorentz and Lorenz [23] expression:

$$R_{LL} = \frac{n^2 - 1}{n^2 + 2} \frac{M}{\rho} \qquad 2\text{-}7$$

where M is the molar mass of the polymer structural unit.

Goedhart [24] made an extensive regression analysis on the group contributions of about a thousand organic liquids, including most common polymers. According to Van Krevelen [21], Goedhart's group contributions approach permit the prediction of the refractive index n with a mean standard deviation of 0.4%.

Most polymers do not absorb electromagnetic radiation in the visible range [21]. The absorption phenomena are related to the excitation energy of molecular bonds. Hence, the light intensity loss due to absorption when using the reflection sensor is expected to remain constant throughout the injection moulding cycle.

The effect of light scattering by particles needs to be considered in experiments with semicrystalline materials. The Mie theory has been used to generate exact solutions to the light scattering by a single particle [25]. The crystallization process inside the mould cavity is a multiple scattering problem, for which no analytical solutions are available. Experimental analysis of the morphology of injection moulded specimens is necessary to obtain information concerning particle geometry during the onset of solidification. Such work is beyond the scope of this research.

Chapter 3

Experimental Procedure

An optical sensor similar to that described by Bur and Thomas in [12,13] was constructed and tested in the injection moulding machine of the Chemical Engineering department at McGill University.

3.1 McGill Injection Moulding Equipment

The injection moulding equipment used during this work was a 60-ton Danson Metalmec machine of the reciprocating screw type. Its general specifications are given in Table 3.1. The original configuration of the machine is described in [26].

Table 3.1 Specifications of the McGill Injection Moulding Machine

Machine Features	Description
Electric Motor	14.92 kW, 3 phase, 60 Hz
Hydraulic Pump (injection unit)	Sperry-Vickers vane pump, 1.82 m^3/hr flow at 13.8 MPa pressure
Clamping Force	60 T (53386 kN)
Capacity	2 1/3 oz (66.1 g)
Screw Diameter	35 mm
Screw L/D Ratio	15
Screw Rotation Speed	40-150 RPM

The McGill IMM has been extensively modified from its original configuration. Previous research work at McGill University has incorporated a control computer and multiple

sensors that are used to monitor the most relevant process variables [27]. Additionally, two servo-valves were installed in the hydraulic system to improve the control capabilities over the hydraulic pressure for the injection moulding unit [28]. A brief description of the main machine components is presented below.

3.1.1. Instrumentation and Hardware

An ALR personal computer (PS/2 compatible) with an i80486DX CPU currently hosts and executes the operation and control software for the injection moulding machine. The computer is connected to two RTI220 data acquisition boards supplied by Analog Devices [29]. Each board can handle a maximum of sixteen inputs and four outputs. The inputs are converted to numeric form before being sent to the computer. One of the boards is used to collect rapidly varying signals such as pressure and screw displacement; this is called the "fast" board. The second board - the "slow" board, is used to collect slowly varying signals, such as temperature.

Digital limit switches that sense the displacement of the movable platen, the carriage and the screw were part of the original instrumentation of the injection moulding machine. As a result of later research, many other sensing devices have been added yielding a highly instrumented machine in its current configuration. Fourteen thermocouples are installed for monitoring temperature in the barrel, mould cavity, and cooling water tubing. Four pressure transducers collect pressure data from the hydraulic line to the injection moulding unit, the nozzle, and the mould cavity. A flowmeter is used to gather flow rate data for the mould cooling water. A velocity transducer is used to measure velocity of the screw. Finally, a linear displacement transducer gathers data concerning the position of the screw. The board and channel to which each sensor is connected are presented in Tables 3.2 and 3.3. The locations of the sensors in the machine are shown in Figure 3.1.

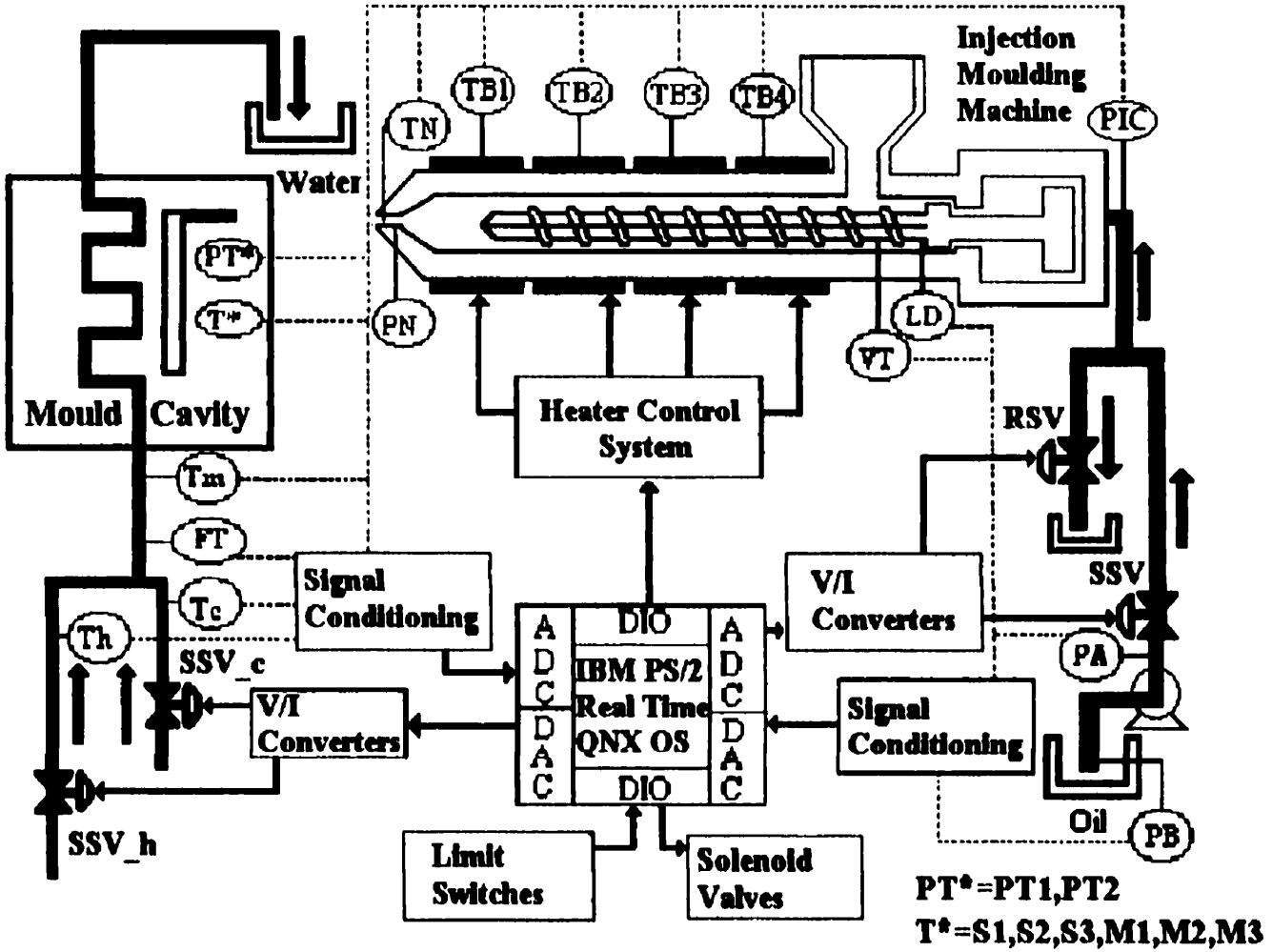

Figure 3.1 Instrumentation of the McGill Injection Moulding Machine. See Tables 3.2 and 3.3 for nomenclature.

An RTI-217 digital I/O board supplied by Analog Devices [30] is used to handle the digital signals that control the solenoid valves of the hydraulic pipeline. A detailed description of the instrumentation and data conditioning can be found in [27].

Table 3.2A Slow ADC card input connections

Channel	Sensor	Description
Input 0	TB1	Thermocouple type E, measures temperature of the zone 1 of the barrel.
Input 1	TB2	Thermocouple type E, measures temperature of the zone 2 of the barrel.
Input 2	TB3	Thermocouple type E, measures temperature of the zone 3 of the barrel.
Input 3	TB4	Thermocouple type E, measures temperature of the zone 4 of the barrel.
Input 4		Not used
Input 5		Not used
Input 6	TN	Thermocouple type K, measures nozzle melt temperature.
Input 7	TH	Thermocouple type E, measures temperature of the hot water used in the coolant system.
Input 8	TC	Thermocouple type E, measures temperature of the cold water used in the coolant system.
Input 9	TM	Thermocouple type E, measures temperature of the mixed water used in the coolant system.
Input 10	FT	Compak 8500 flow transmitter. Measures flow rate of the cooling water.
Inputs 11-15		Not used.

Table 3.2B Slow ADC card output connections

Channel	Device	Description
Output 1-2		Not used
Output 3	Ssv	Supply servovalve Moog A076-103. Regulates the oil flow to the injection cylinder.
Output 4	Rsv	Relief servovalve Moog A076-103. Regulates the flow of oil returning to the tank.

Table 3.3A Fast ADC Card Input Connections

Channel	Sensor	Description
Input 0	PT1	Pressure transducer LTD GP-50 132. Measures pressure at the gate of the cavity (0-34.7 MPa).
Input 1	PIC	Pressure transducer Dynisco 432A-1M. Measures pressure at the injection cylinder (0-27.6 MPa).
Input 2	PN	Pressure transducer Dynisco PT435 A-10M. Measures pressure at the nozzle (0-68.94 MPa).
Input 3	PA	Pressure transducer Dynisco PT434-3M. Measures pressure after the oil pump (0-27.57 MPa).
Input 4	PB	Pressure transducer Dynisco PT434-3M. Measures pressure before the oil pump (0-27.57 MPa).
Input 5	PT2	Pressure transducer Dynisco PT435 A-3M. Measures pressure at the cavity center (0-27.57 MPa). Not used.
Input 6	S1	Eroding type E NANMAC thermocouple. Measures surface temperature near the cavity gate.
Input 7	S2	Eroding type E NANMAC thermocouple. Measures surface temperature near the middle of the cavity.
Input 8	S3	Eroding type E NANMAC thermocouple. Measures surface temperature near the far end of the cavity.
Input 9	M1	Custom made thermocouple type E. Measures mould metal temperature near the cavity gate.
Input 10	M2	Custom made thermocouple type E. Measures mould metal temperature at the middle of the cavity. Not used.
Input 11	M3	Custom made thermocouple type E. Measures mould metal temperature near the far end of the cavity.
Input 12,13		Not used.
Input 14	LD	Linear displacement transducer Temposonics model no. 011012070208. Measures screw displacement.
Input 15	VT	Velocity transducer Temposonics model no. 321001008 RCU 0120. Measures screw velocity.

Table 3.3B Fast ADC Card Output Connections

Channel	Device	Description
Output 1	Cv_c	Cold water servovalve PCT model 1/2-B-EQ. Regulates the cold water flow rate.
Output 2	Cv_h	Hot water servovalve PCT model 1/2-B-EQ. Regulates the hot water flow rate.
Output 3-4		Not used.

3.1.2. Operation and Control Software

The injection moulding machine is operated and controlled with the execution of the "*imm*" program. *imm* is primarily an interface developed by Fusser and Gao [31,27] which schedules the execution of other processes. These processes are other programs that gather data, process information, and issue commands according to the sequence of the injection moulding cycle, to control the machine operation. The execution of such processes is transparent to the user. The *imm* interface facilitates the interaction by requesting from the user to only specify the operating conditions for the machine. The following information is required:

- File names for storage of data collected by the two ADC boards.
- Settings for timers of the injection, holding and cooling stages.
- Sampling rates for each channel of the ADC boards, in function of each stage of the injection moulding cycle.
- Channels to sample from each board (i.e. temperatures, pressures, etc.).
- Barrel temperature profile.
- Mode of operation: automatic, semi-automatic or manual.

All programs are written in the C programming language, using a compiler and libraries supplied by Watcom [32] that include real-time extensions for the QNX operating system. A detailed description of the operation software can be found in [27,31]. The operating system is QNX 4.1, supplied by QNX Software Systems Ltd. [33]. QNX is a real-time multitasking operating system based on Unix, designed to run in PC compatible computers.

3.2 Construction of the Optical Sensor

The basis of the optical sensor is the change in optical characteristics of the polymer as it solidifies, as discussed in §2.3. The most important effects on the light beam were

expected to be caused by the reflection of light at the polymer/cavity walls, the reflection at the opposite wall of the mould, and scattering and refraction while the light beam traverses the specimen. The sensor was therefore designed so that the effects expected due to melt solidification caused measurable variations in the detected light intensity, as will be discussed in §3.2.1. The mechanical restrictions for the installation of the sensor in the injection moulding machine determined the components for the sensor.

3.2.1 Sensor Design

The sensor operation requires illuminating the melt inside the mould cavity using a light source of appropriate wavelength, collecting the reflected light, and measuring the reflected intensity. The trajectory for the illuminating and reflected beam is shown in Figure 3.2.

The light source chosen was a 0.5 mW Helium-Neon laser supplied by Optikon [34]. The wavelength of He-Ne lasers is 632.8 nm. Radiation in the visible range is convenient because it is known that most polymers show very little absorption for such wavelengths. Hence, the absorption phenomenon would be reduced. Since laser radiation is monochromatic, discarding of unwanted radiation in the detection equipment using a bandpass filter is facilitated. The other sources of radiation are the hot specimens inside the mould cavity, which generate IR radiation that may also be detected by the sensing instrument.

One of the branches of a dual branch fiber optic bundle A53045 supplied by Edmund Scientific [35] was chosen as light guide from the laser tube to the mould cavity. The second branch of the light guide delivers the reflected light from the cavity to the detection equipment. This is a critical component, as its flexibility allowed easy installation on the movable platen of the injection moulding machine. Ordinary focusing devices such as lenses and prisms need sophisticated mounting and careful alignment.

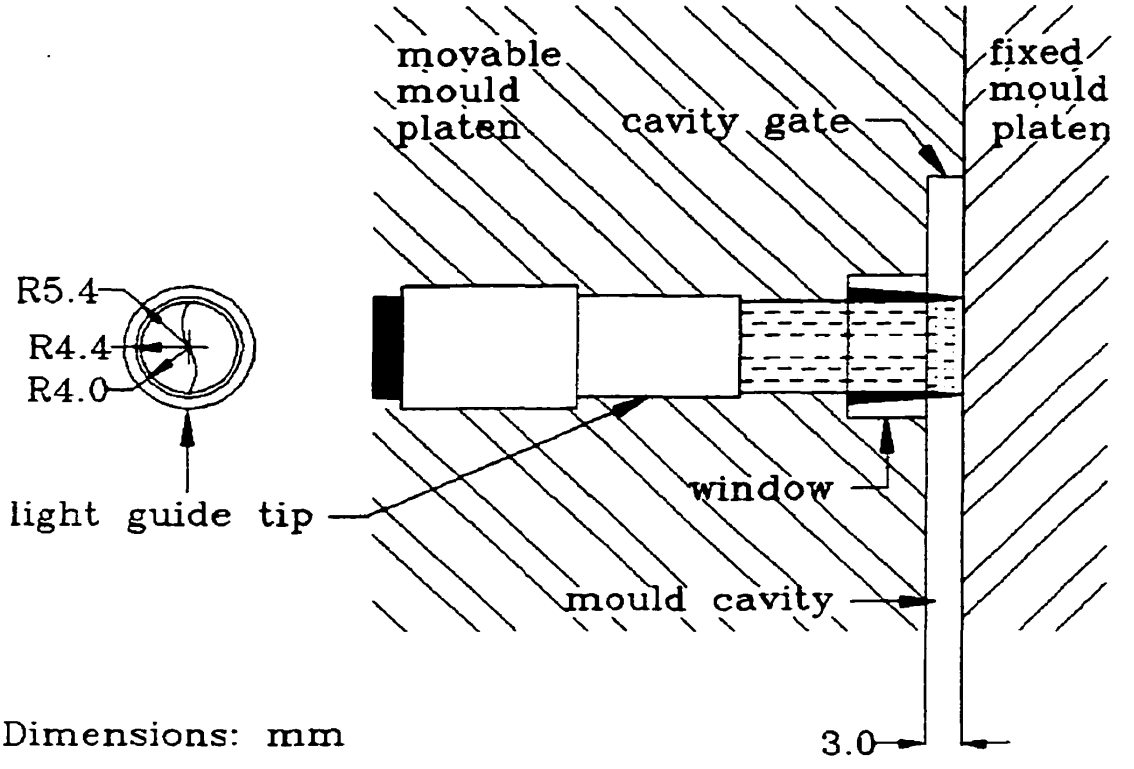

Figure 3.2 Installation of light guide and window on the movable mould platen. R4.0 corresponds to the fiber bundle radius (inner circle); R4.4 is the radius of a metal bundle sheath (middle circle), and R5.4 is the radius of a metal ferrule (external circle).

However, the geometry of the IMM platens considerably limits the space available for other devices that can be mounted.

The light is allowed to pass into the mould cavity through a fused silica window installed on the mould insert. Figure 3.3 shows the position of the window on the insert. It was decided that an appropriate position would be near the cavity gate. The solidification takes longer to complete in this region and thus longer observation periods would be available during each injection moulding cycle. CVI Laser supplied the optical window. Its transmittance at 632.8 nm is approximately 90 % [36].

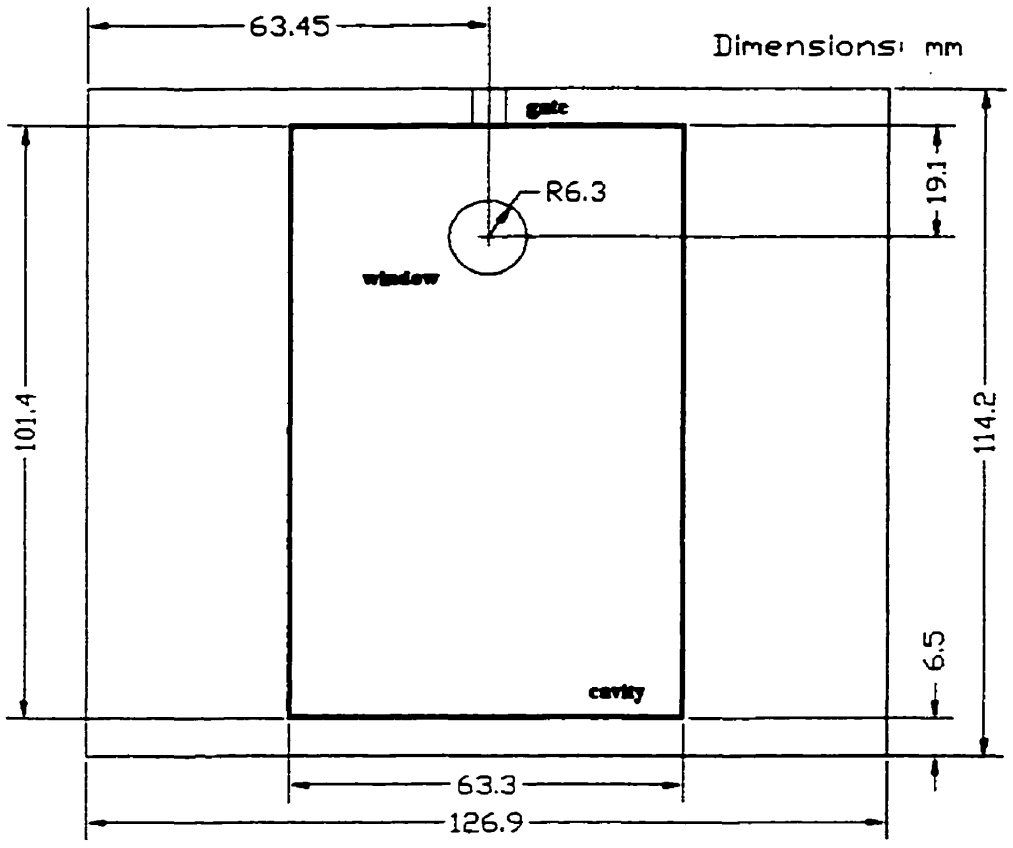

Figure 3.3 Position of the window on the mould insert

Reflected light was detected by a Photomultiplier Detection System model 7070 supplied by Oriel Corp. [37]. This is a photoemissive detector in which light directly interacts with the electrons in the detector material. The absorbed photons eject electrons from a photocathode in the instrument. An applied voltage causes the electrons to flow towards an anode, creating a current that is proportional to light intensity over 6 to 8 orders of magnitude. Photomultipliers are more sensitive than any other detector in the near UV and visible regions of the spectrum. A He-Ne laser bandpass filter supplied by Oriel [38] was used to eliminate light of unwanted wavelengths from the signal. The photomultiplier provides an analog output voltage that is input to the data acquisition board.

3.2.2 Sensor Installation

The installation of the fiber optics light guide for illumination of the optical window required the construction of a special adapter. This was necessary to keep the fiber optics bundle fixed in place, focused at the same point of the optical window throughout the injection moulding cycle. The light guide was installed on the movable platen because several pressure transducers and thermocouples already crowd the fixed platen surface. The installation was also easier because the disassembly and remounting of the fixed platen requires great care to not damage the existing sensors. The adapter positioned the tip of the light guide less than three cm away from the optical window. A second adapter was installed in the platen to contain a leak from one of the cooling channels which was caused during the enlarging of a hole though the platen required to install the light guide.

A mould insert was drilled to install the optical window in the position shown in Figure 3.3. The window was fixed in place using Milbond, an elastomeric-epoxy adhesive system for glass to metal applications, supplied by Summers Optical [39].

The light guide was coupled to the laser tube using a set of standard optical adapters supplied by Edmund Scientific [35]. The connection of the light guide to the detection equipment required another set of adapters and a filter holder from Oriel Corp. [38], because the bandpass filter had to be positioned between the tip of the light guide and the photomultiplier tube opening. Figure 3.4 shows the complete optical system as it was finally installed on the injection moulding machine.

The output signal from the photomultiplier amplifier was connected to channel 12 of the "fast" ADC board. The signal was expected to vary rapidly during the packing phase of the injection moulding cycle, in proportion to the solidification rates of the materials used in experiments. The sampling rates and other machine settings are described in Appendix A.

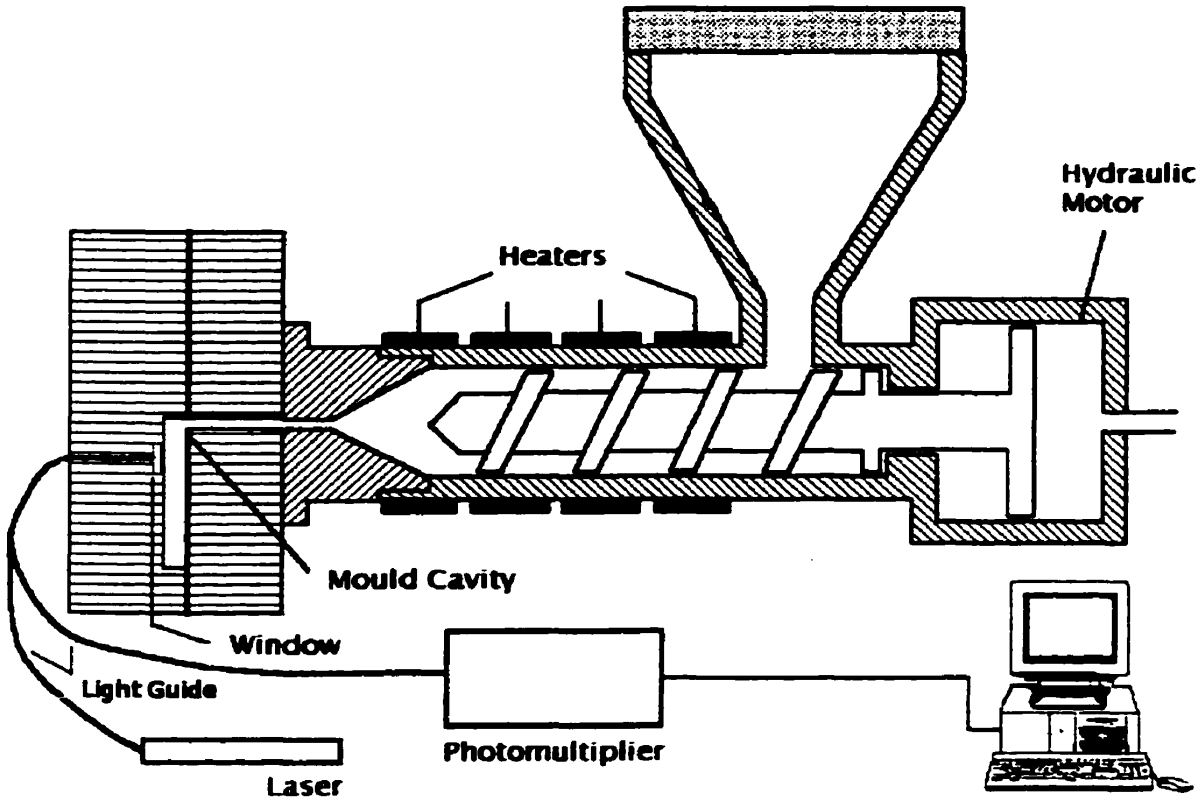

Figure 3.4 Optical sensing apparatus installed on the injection moulding machine

3.3 Materials

The materials used in the experimental work were:

- High-density polyethylene (HDPE) Sclair 2908 supplied by Nova Chemicals [40]. The crystallinity of for injection moulded Sclair 2908 HDPE has been found to be 60-70 % [41].
- Polypropylene (PP) Profax 6523 supplied by Himont (now Montell) [42]. This isotactic polypropylene resin exhibits crystallinity values of approximately 60 % or less [41].
- Polystyrene (PS) Styron 685D supplied by Dow Plastics [43]. This is an amorphous resin.

The scattering effect was expected to be stronger for semi-crystalline polymers than for amorphous materials. During solidification the formation of crystalline structures in semi-crystalline materials promotes a stronger effect of scattering by particles. Other relevant data for the materials used are presented in Table 3.4.

Table 3.4. Physical properties of the materials used in experiments

Property	Polyethylene Sclair 2908	Polypropylene Profax 6523	Polystyrene Styron 685D
Solid Density	0.96 g/cm^3	0.90 g/cm^3	
Melt Index	7.3 dg/min		
Bulk Density	0.61 g/cm^3		0.59 g/cm^3
Melt Flow Rate		4 g/10 min	1.6 g/10 min
Softening Point (Vicat)	129 °C		108 °C

3.4 Measurement Procedure

The measurement of the absolute magnitude of the reflected intensity was not necessary in this study. The photomultiplier operates in relation to a reference value. Hence, relative values of the reflected intensity were determined. The intensity value measured at the beginning of the injection moulding cycle was used for the normalization of the intensity scale. No absolute calibration was needed. The photomultiplier was used above its noise equivalent power (NEP) value, and below the damage level [37]. NEP is the radiant flux necessary to give an output equal to the noise output from the detector. The instrument used has a NEP of 0.053×10^{-8} A. The damage level of the photomultiplier is 10^{-5} A.

The intensity scale was normalized using two reference values, taking care not to reach the damage level of the photomultiplier. The reflected intensity references were two orders of magnitude above the NEP. Considering that the photomultiplier amplifier covers only an order of magnitude without switching, the zero value for the normalization

was 10^{-7} A. The excitation voltage was set to 422 V so that the intensities measured during the experiments were between 10^{-7} and 10^{-6} A. The output was linear. The intensity recorded for the empty, closed mould was taken as the reference value 1 for the normalized scale.

A characteristic curve was obtained from the measurements of reflected light intensity for all experimental conditions and resins. Its relevant points and the interpretation of trends are presented in Chapter 4.

Preliminary experiments showed that the technique depends on environmental conditions. Changes in environmental temperature and humidity caused the laser intensity detected with the photomultiplier to vary. Hence, care was taken to perform experiments under approximately the same environmental conditions. It was also noticed that the laser used needs an initial warm up period before settling on stable intensity levels. Reproducibility was achieved once these factors were controlled.

Chapter 4

Measurements and Analysis of Reflection Intensity during the Injection Moulding Cycle

The performance of the sensor was tested using three different materials: polyethylene, polypropylene and polystyrene. A set of experiments at different mould pressure and temperature conditions was performed for each material. The reflection intensity data collected were processed and analyzed. The reflection intensity profiles obtained were explained using a model that partially reproduces the most relevant phenomena affecting light transmission through the moulded specimens.

4.1 Characteristics of the Reflection Intensity Curve

The reflection intensity data obtained during the experiments were plotted against time. The relevant process variables were also plotted to visualize characteristic points in the cycle. Thus the plots include data for cavity pressure, nozzle pressure, and cavity temperature. A typical plot of reflected light intensity, cavity pressure and nozzle pressure is presented in Figure 4.1.

A characteristic shape was observed for the intensity curve in every experiment performed, regardless of whether the material used was semicrystalline or amorphous, or what the pressure and temperature processing conditions were. The interpretation for the trend changes of this characteristic curve is as follows. The initial light intensity measurement is 1, which corresponds to the normalized value for reflection from the closed, empty mould at the beginning of the cycle. When the mould is filled, the intensity values immediately decrease. The end of filling of the mould cavity is recognized by the sudden increase in cavity pressure, which also denotes the beginning of the packing stage. The rate of intensity decrease changes with time during this period. Initially, the intensity

decreases quickly, but the rate slows down gradually, until a plateau is obtained, where the lowest intensity values are recorded. In Figure 4.1 the intensity minimum occurs between 15 and 20 seconds.

According to the cavity pressure profile, the polymer is still in contact with the mould walls during this period. The fact that the cavity pressure remains high implies that more melt is being injected from the injection unit. The wall temperature values recorded on the surface are below 80 °C, in concordance with data reported in [44]. This implies that the polymer in contact with the wall has solidified. Therefore, the solidification process is still continuing, and the sensing conditions are most favorable for the operation of the reflection intensity sensor, as there are no air interfaces between the window and the polymer in the cavity. The line that intersects both curves at 18 seconds marks the minimum reflection intensity value, which coincides with the point of the cavity pressure curve corresponding to the freezing of polymer in the cavity gate. This issue is discussed in §4.3.

After reaching the minimum, the reflection intensity curve increases slightly for 10 seconds, until a sharp change in the curve is recorded at 30 seconds. There, the intensity suddenly increases to values above the normalized value 1. This abrupt change is caused by the separation of the polymer from the mould walls. The reflection from the polymer specimen to the window is responsible for this sudden variation of intensity values. When the polymer shrinks away from the mould wall, air fills the space between window and polymer. The reflection intensity is stronger at the air-polymer interface than at the window-polymer interface, due to the smaller value of the refractive index of air compared to the refractive index of fused silica, according to Fresnel's equation (eq. 2-4).

For the rest of the cycle, the intensity curve remains at high values, while the specimen is still inside the mould cavity. Later, when the specimen is ejected from the mould, the reflection intensity decreases again. At this point the nozzle pressure curve shows higher values, approximately at 49 seconds, due to the activity of the hydraulic system which causes opening the mould and retraction of the carriage. The cycle is completed when the

mould closes in preparation for the next cycle, and the reflection intensity value reaches the normalized value "1" again.

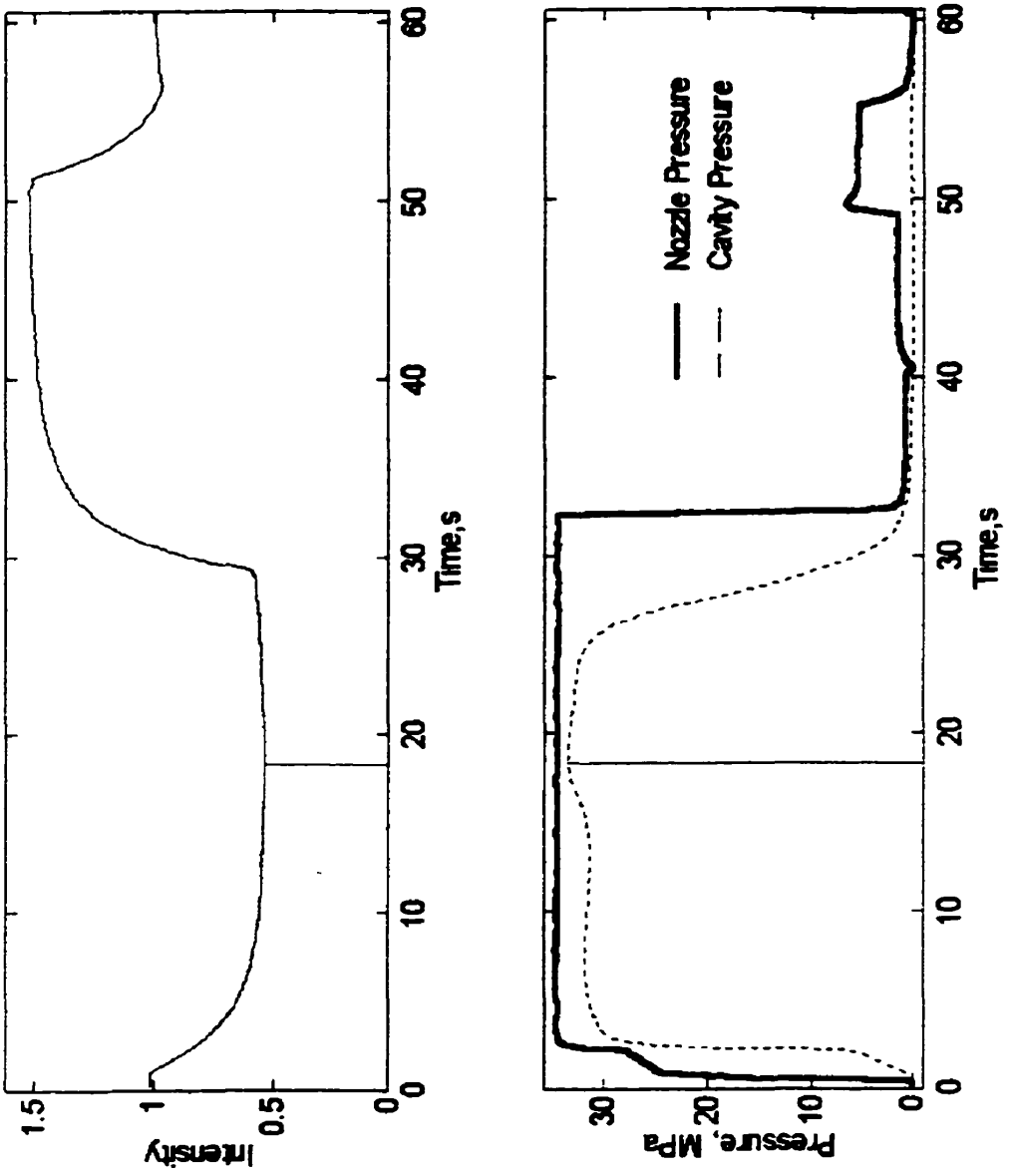

Figure 4.1 Typical plots for reflection intensity and pressure, for injection moulding of HDPE. The cooling water temperature was maintained at 25°C.

4.2 Summary of Experimental Tests on the Sensor Performance

The optical sensor was tested under different operating situations that were expected to cause some modification of the characteristic output. The three resins allowed the collection of data on solidification processes under different crystallization conditions. Table 4.1 presents a summary of the main experiments and relevant machine settings and process variables. The label is used to associate data in the table with the corresponding figure.

Table 4.1 Summary of the tests to analyze the sensor performance. Tc refers to temperature of cooling water, in °C. SSV refers to the percentage of opening of the supply servovalve, Pn refers to the nozzle pressure, in MPa.

Experiment	Label	Tc, °C	SSV, %	Pn, MPa
High Cooling Temperature	HDPE/HT	48	60	38
	PP/HT	63	60	38
	PS/HT	47	60	38
Low Cooling Temperature	HDPE/LT	7	60	37
	PP/LT	7	60	38
	PS/LT	7	60	38
High Packing Pressure	HDPE/HP	24	80	38
	PP/HP	24	80	38
	PS/HP	25	80	38
Low Packing Pressure	HDPE/LP	24	40	25
	PP/LP	25	40	30
	PS/LP	24	40	28

For each resin, experiments were performed setting the cooling water temperature to different values, so different cooling rates were evaluated. Similarly, different experiments for each resin were performed to examine the sensor response at different packing pressure values. The supply and relief servovalves of the hydraulic unit were manipulated to achieve different packing pressures.

4.3 Material Influence on Transmission of Light across the Specimen

The reflection intensity curves obtained for each material show differences when compared to typical profiles of the two other materials. Figure 4.2 presents typical reflection intensity curves for specimens of the three materials. It is seen that the largest light scattering effect is caused by polyethylene. The polyethylene (HDPE) and polypropylene (PP) resins used are both semi-crystalline materials, but the crystallinity of HDPE is approximately 70%, whereas for PP the crystallinity is 60%. The polystyrene (PS) plot shows even less difference between the reflection intensity readings for empty and filled mould. The PS resin used is an amorphous material, for which the scattering effects are the smallest.

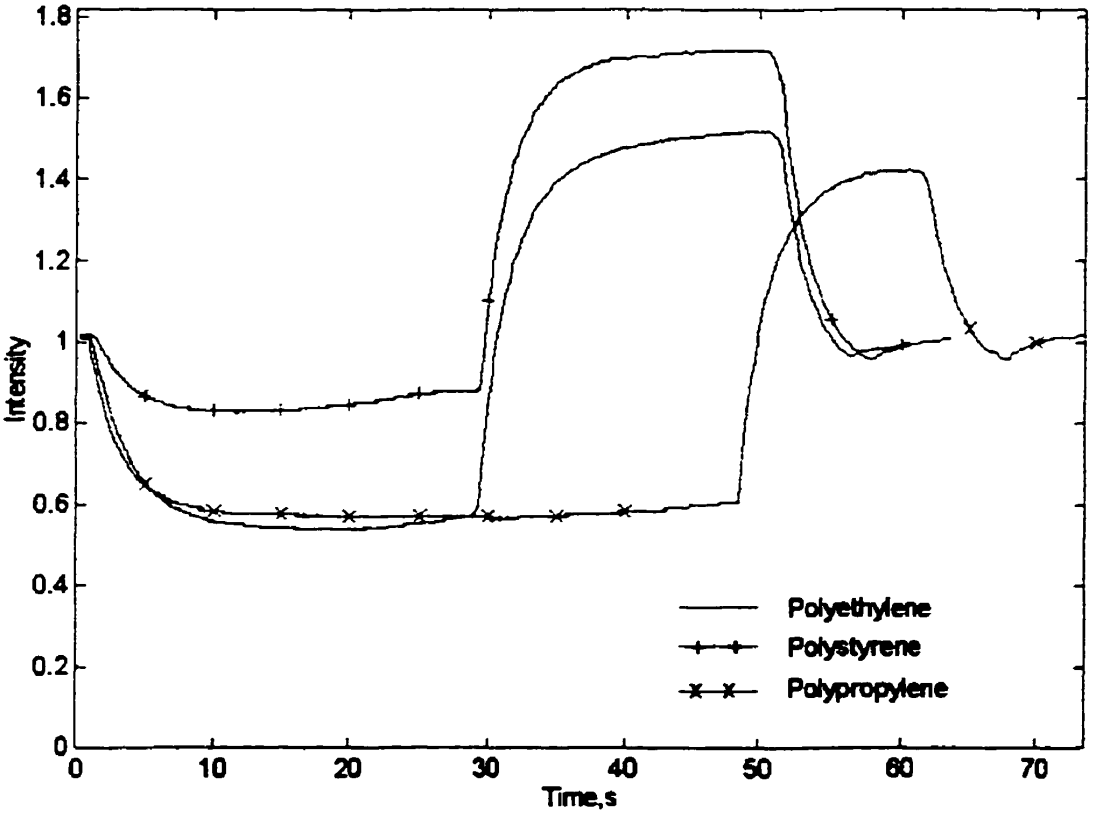

Figure 4.2 Comparison of reflection intensities for polyethylene, polypropylene, and polystyrene.

The influence of the degree of crystallinity on light transmission across the specimens derives from the scattering power of crystalline structures and spherulites formed upon solidification. Semi-crystalline materials never solidify into completely crystalline solids [8]. Instead, there always remain amorphous regions filling the spaces between crystalline structures. The presence of amorphous and crystalline material intermixed in the morphology of solid specimens implies that there are multiple interfaces between crystalline and amorphous material in a single sample. Therefore, the light beam traveling across such morphology experiences strong scattering compared to a single phase.

A reduction in the intensity of transmitted light was also observed in the case of the amorphous polystyrene resin used. The reduction in light intensity is smaller than for polyethylene and polypropylene due to the absence of crystalline structures. Figure 4.2 shows that the final intensity for light transmitted through the PS specimen after 30 seconds, just before the specimen separates from the walls, is approximately 0.9. The intensity for PP and HDPE is 0.6 at the same time.

Figure 4.2 also shows that, after the injection moulded specimens have separated, the intensity values for the PS curve remain higher than for PP and HDPE. In §4.1 it was mentioned that the high intensity measured in this period of the IM cycle is caused by reflection from the specimen wall in front of the window. While the PP and HDPE curves are at similar levels, the difference recorded for the PS curve may be explained in terms of the differences of refractive indices values. From equation 2-4 follows that larger values of refractive index cause larger reflectance. The refractive indices of PP and HDPE are similar and both are smaller than the refractive index of PS, as shown in Table 4.2.

Table 4.2 Refractive indices of the solid materials used in experiments, taken from [20]. The values for amorphous polymer melts are estimated according to [24].

Material	HDPE	PP	PS	Fused silica
Refractive index	1.49	1.512	1.591	1.457

A simple observation of the solid HDPE, PP, and PS specimens reveals a decreasing degree of opacity, in that order. The HDPE specimens are opaque, the PP samples are translucent, and the PS specimens are almost transparent. The relative roughness on the surface of the mould walls is responsible for the lack of complete transparency of the PS specimens. The high concentration of crystalline material in HDPE has the highest scattering power, and explains why the smallest values of reflected light intensity after solidification are obtained in this case. The highest intensity values are obtained in the PS plots, whereas the PP plots show intermediate positions between the HDPE and PS ranges.

4.4 Effects of Pressure Changes on Transmission of Light across the Specimens

A set of experiments for each material was performed to observe how different cavity pressure values affect the intensity of light reflected from the cavity during the packing stage. Figures 4.3, 4.4, and 4.5 show the curves for polyethylene, polypropylene and polystyrene, respectively.

In §4.1 it was mentioned that a correspondence between the minimum of intensity values and the cavity pressure values was detected: a change in the slope of the cavity pressure curve is observed at this time. This point of the cavity pressure curve corresponds to the moment when the cavity gate freezes. After this time, no more melt is allowed into the cavity, and the pressure inside the cavity decreases at a faster rate. The curve for polyethylene is the clearest. In Figure 4.3A the moment when the cavity gate freezes is 19 seconds. In the polypropylene and polystyrene curves (Figures 4.4A and 4.5A), the gate freezes at 25 and at 14 seconds, respectively.

From the high-pressure experiments, it can be appreciated that the intensity begins to decrease slightly earlier than in the lower pressure experiments. This occurs as a consequence of the additional mass of polymer injected into the cavity in the high-pressure experiments. More scattering is observed due to the increased material mass

inside the mould, compared to the lower-pressure experiments. It can also be appreciated that the separation of the polymer from the mould wall occurs later for high-pressure conditions. This effect is also related to the larger mass that frees less space when shrinkage occurs. The delay in the separation from the mould wall is caused by the presence of additional polymer melt forced into the cavity in the high pressure experiments, compared to the low pressure cases. The earlier beginning of scattering and the later separation from the wall indicate a larger cycle for the higher-pressure experiments. The intensity minimum occurs approximately at the same time in the high and low-pressure experiments. Table 4.3 presents the times when the characteristic points occur in the reflection intensity curves.

Table 4.3 Times of occurrence of the characteristic points of the reflection intensity curve for experiments with changing pressure conditions.

Experiments		Intensity decrease	Intensity minimum	Separation from the wall
HDPE	LP	2s	18s	28s
	HP	1	17	30
PP	LP	1	24	42
	HP	1	33	61
PS	LP	2	14	27
	HP	3	13	35

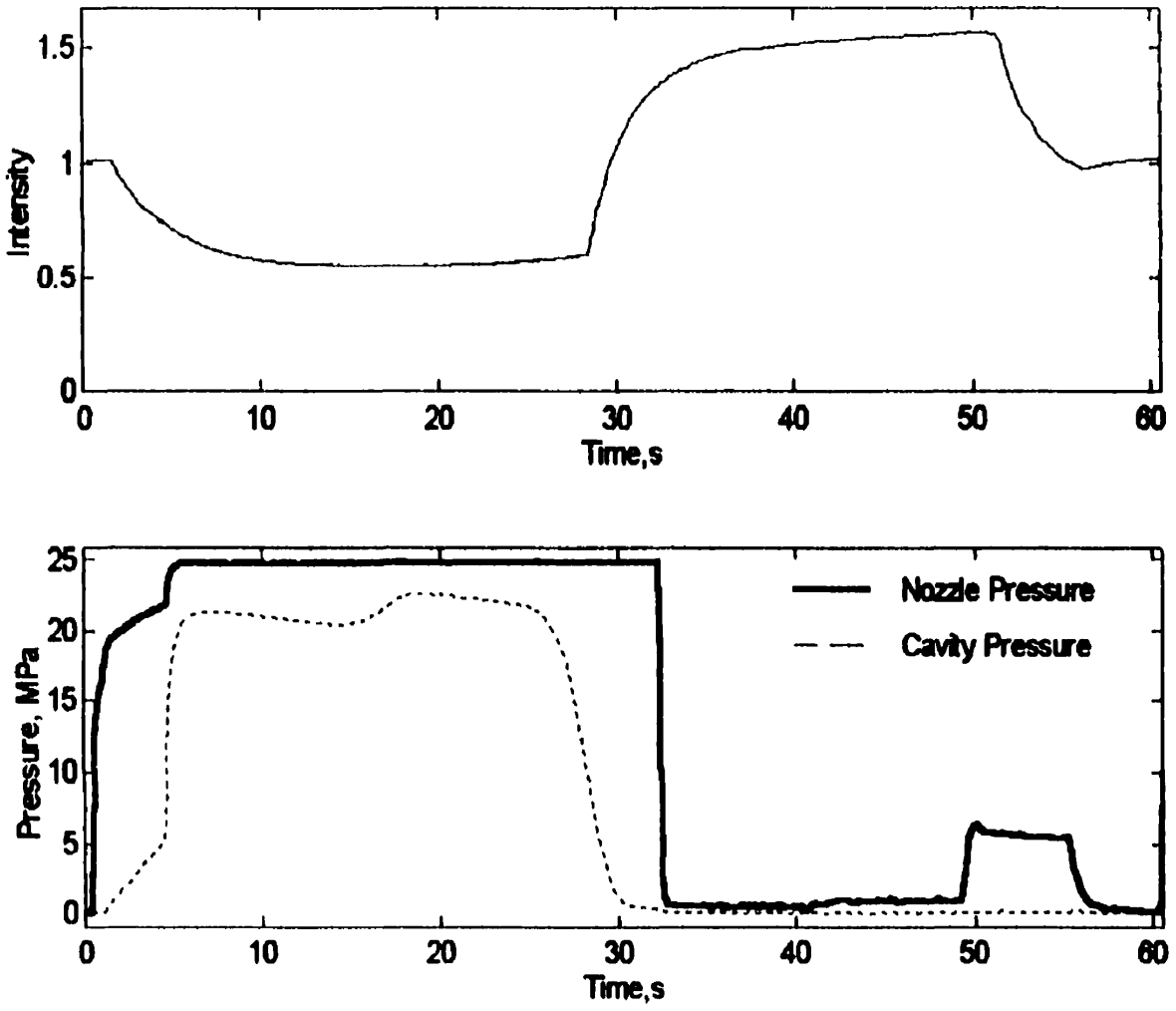

Figure 4.3A Plots of reflection intensity and pressure for HDPE, low pressure experiment - HDPE/LP

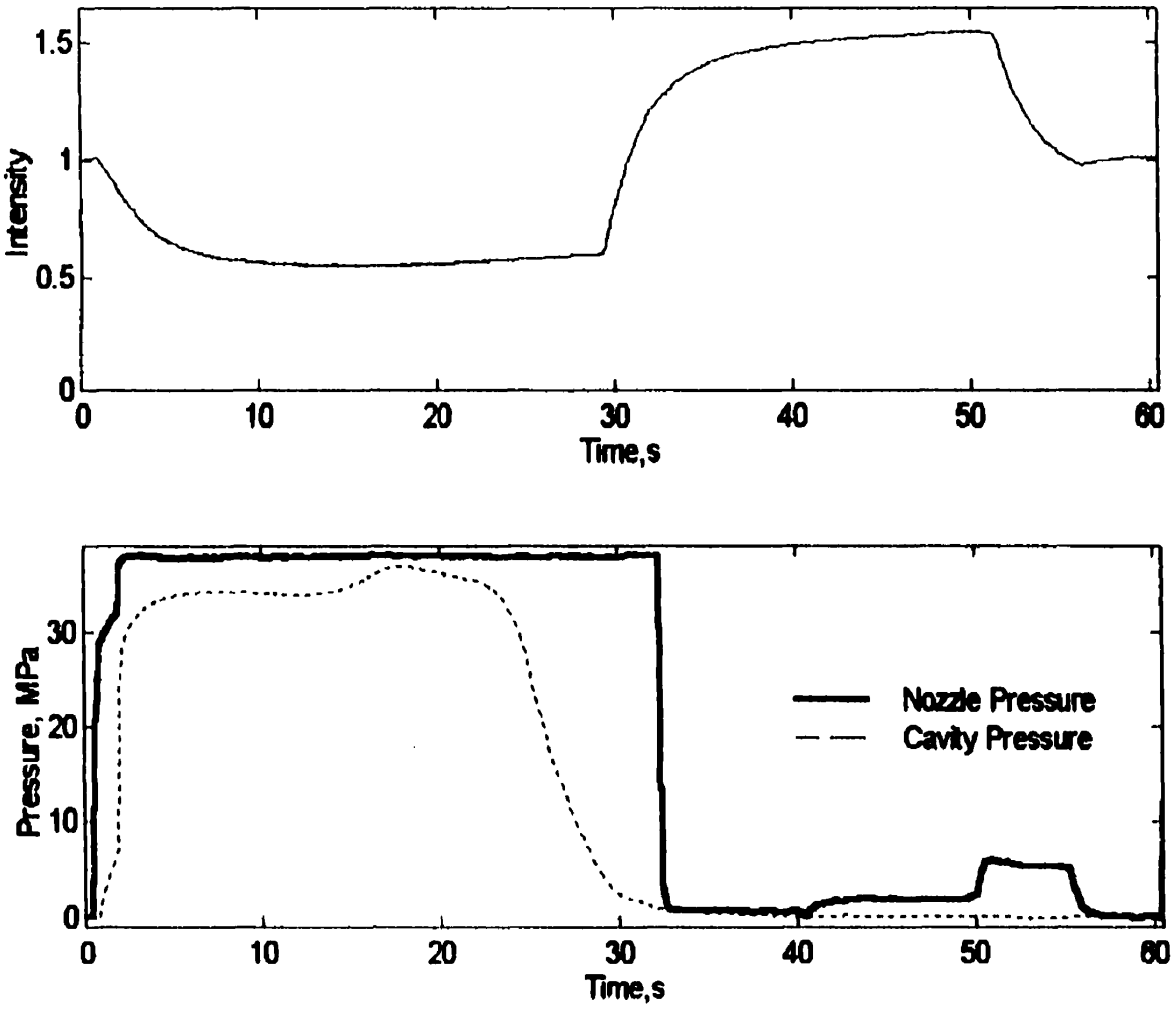

Figure 4.3B Plots of reflection intensity and pressure for HDPE, high pressure experiment - HDPE/HP

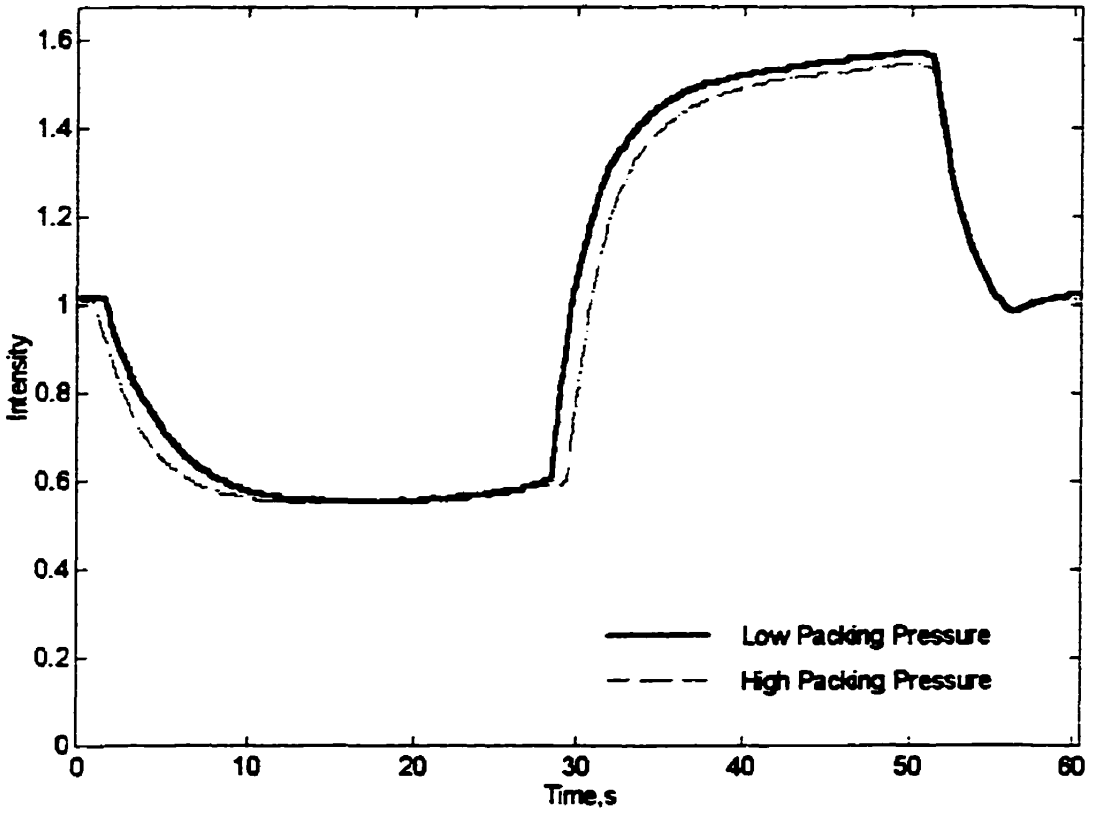

Figure 4.3C Comparison of intensities from the HDPE/LP and HDPE/HP experiments

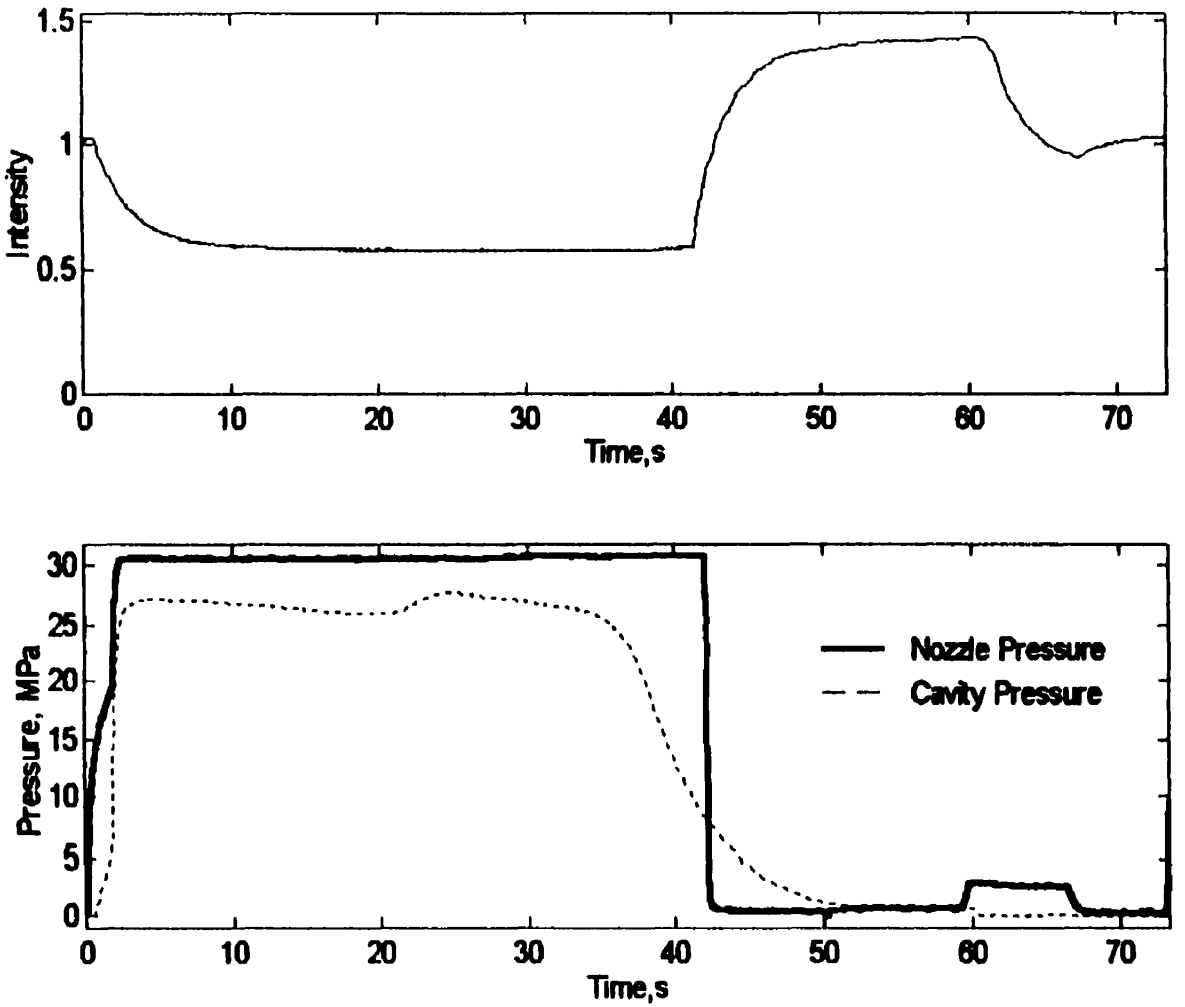

Figure 4.4A Plots of reflection intensity and pressure for polypropylene, low pressure experiment - PP/LP

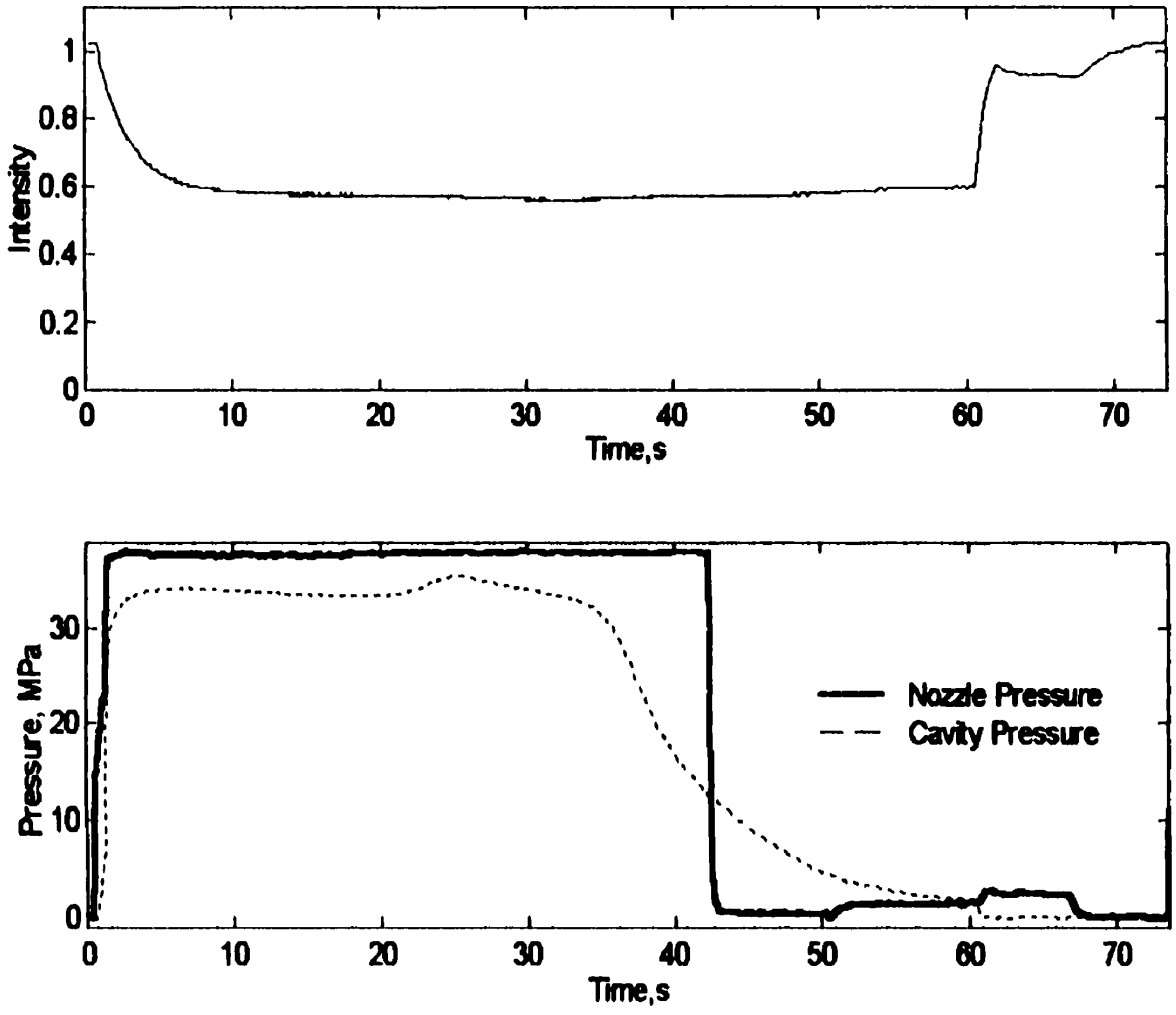

Figure 4.4B Plots of reflection intensity and pressure for polypropylene, high pressure experiment - PP/HP

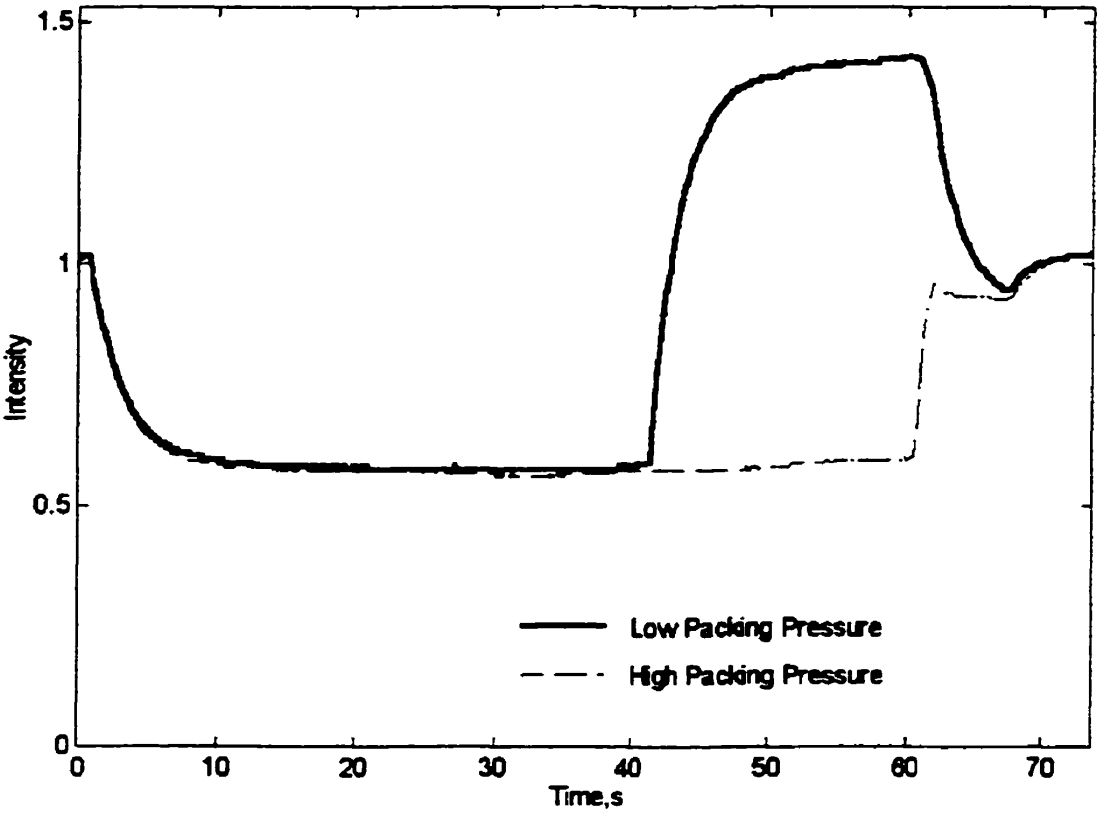

Figure 4.4C: Comparison of intensities from the PP/LP and PP/HP experiments

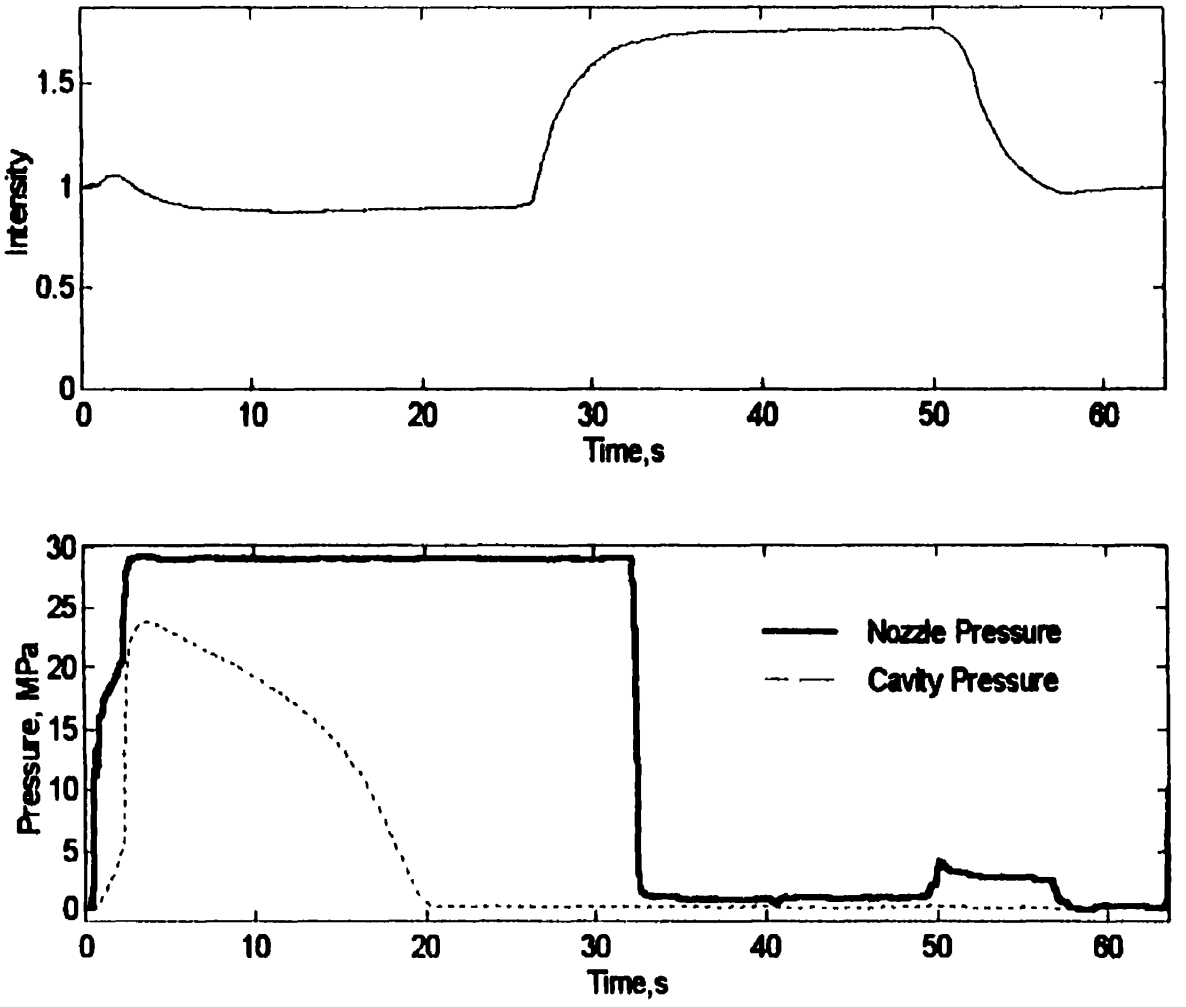

Figure 4.5A Plots of reflection intensity and pressure for polystyrene, low pressure experiment - PS/LP

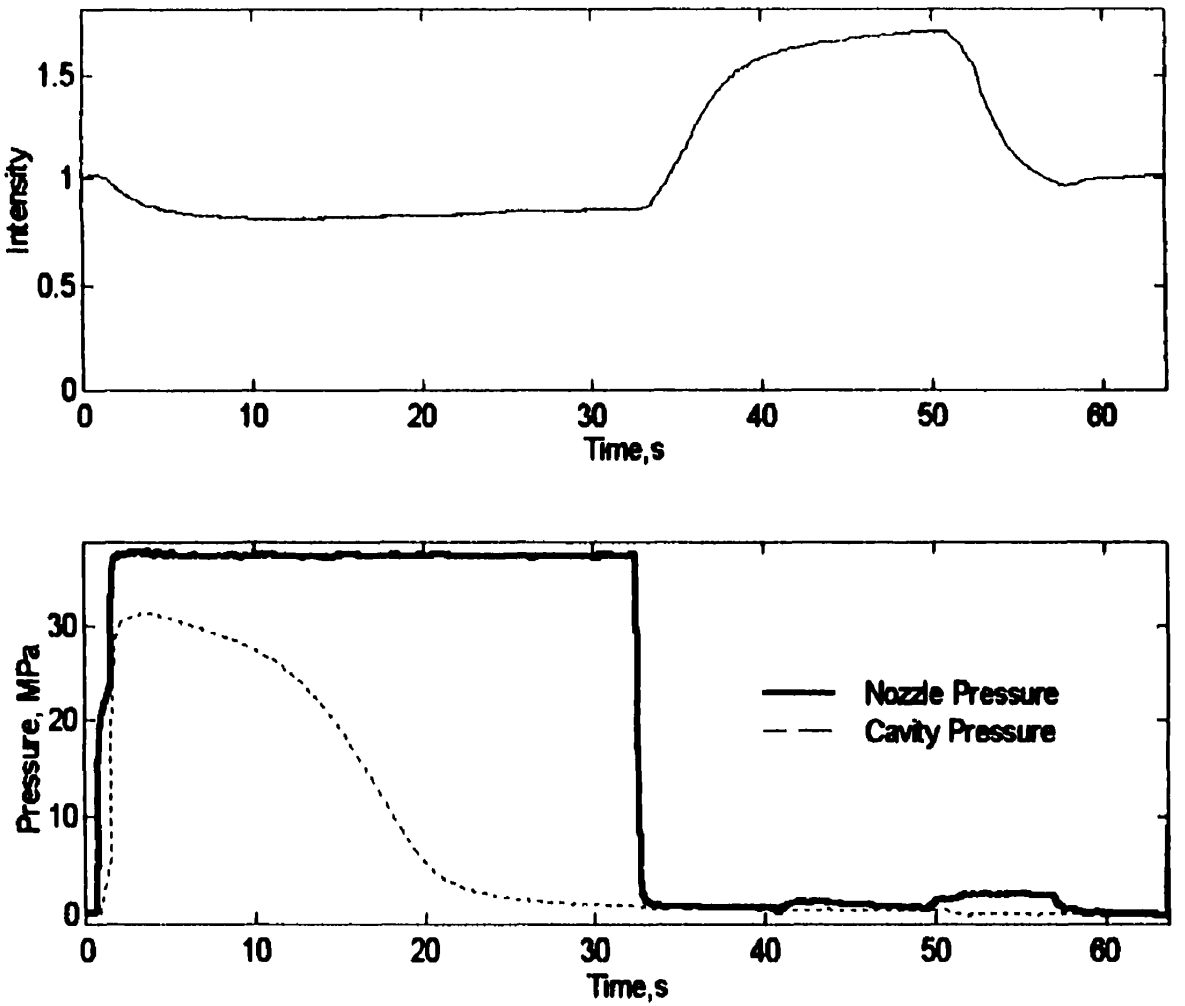

Figure 4.5B Plots of reflection intensity and pressure for polystyrene, high pressure experiment - PS/HP

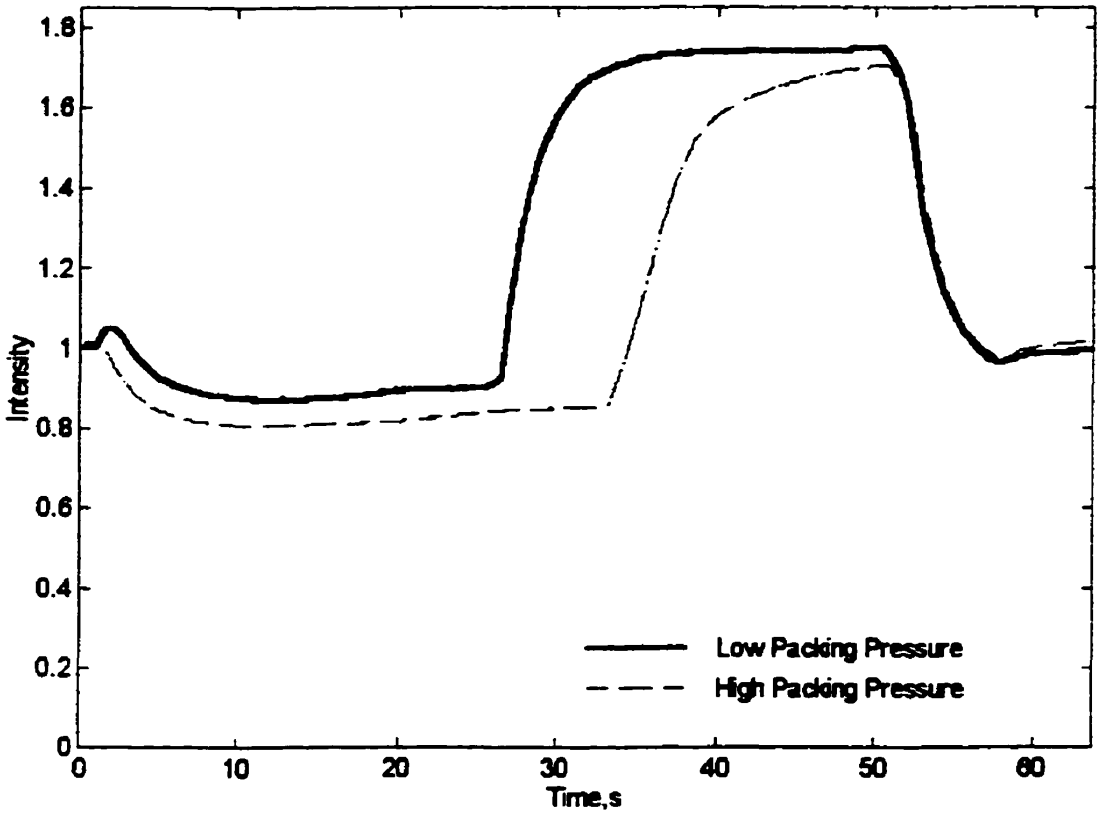

Figure 4.5C Comparison of intensities from the PS/LP and PS/HP experiments

The three sets of curves show similar profiles. The differences are caused by the influence of the material that determines different times and magnitudes of the characteristic points of the curves (e.g. gate freezing, separation from the window). The changes in the curves caused by different materials are described in §4.3.

4.5 Effects of Temperature Changes on Transmission of Light across the Specimen

Different mould temperature settings were used to observe the effects on the transmission of light across solidifying specimens. The plots in Figures 4.6, 4.7 and 4.8 show reflection intensity, cavity pressure, and mould temperature data of the polyethylene, polypropylene

and polystyrene experiments. The mould temperature was controlled by manipulating the cooling water temperature.

In the experiments with low mould temperature, the reflection intensity profile indicates that the solidification process occurs faster than in the experiments with the higher mould temperature. In these experiments, the cooler mould causes the polymer near the walls to cool down and shrink faster, compared to the cases when the mould is warmer. Hence, the polymer in the cavity gate freezes earlier in the cold mould experiments than in the hot mould cases. As with the other characteristic points of the reflection intensity curve, the minimum value of reflection intensity appears earlier when the mould temperature is lowered. Table 4.4 presents the times when the reflection intensity minimum and separation from the wall occur in every experiment.

Table 4.4 Times of occurrence of the characteristic points of the reflection intensity curve for experiments with changing temperature conditions.

Experiments		Curve Minimum	Separation from wall
HDPE	LT	16 s	27s
	HT	21	36
PP	LT	23	44
	HT	37	62
PS	LT	11	26
	HT	13	50

Figures 4.7C and 4.8C show other difference between the reflection intensity curves obtained in the low and high cooling temperature experiments of polypropylene and polystyrene. For both materials the intensity values for the high cooling experiments remain approximately constant for most of the cycle, whereas for the low cooling experiments it may be appreciated that the intensity rises sharply at the end of the packing stage. Hence, in the high temperature experiments the injection moulded part did not separate from the optical window before being ejected from the mould. This phenomenon is attributed to slower shrinkage of the specimens due to the higher temperature. The HDPE specimens always shrank rapidly enough to separate from the optical window. This is caused by the higher crystallinity of HDPE, compared to PP. Amorphous polystyrene experiments less shrinkage than PP and HDPE.

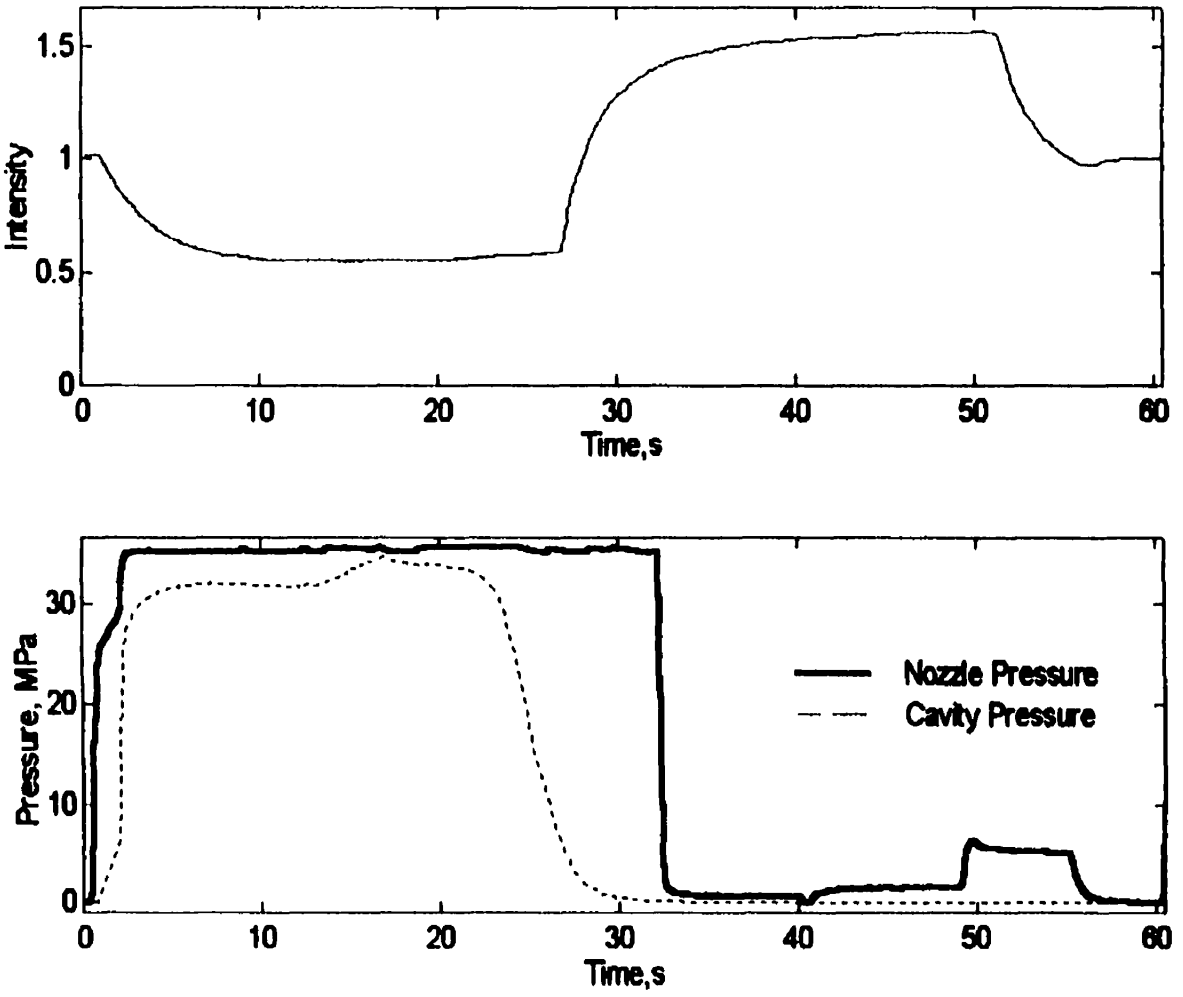

Figure 4.6A Plots of reflection intensity and pressure for HDPE, low cooling temperature experiment - HDPE/LT

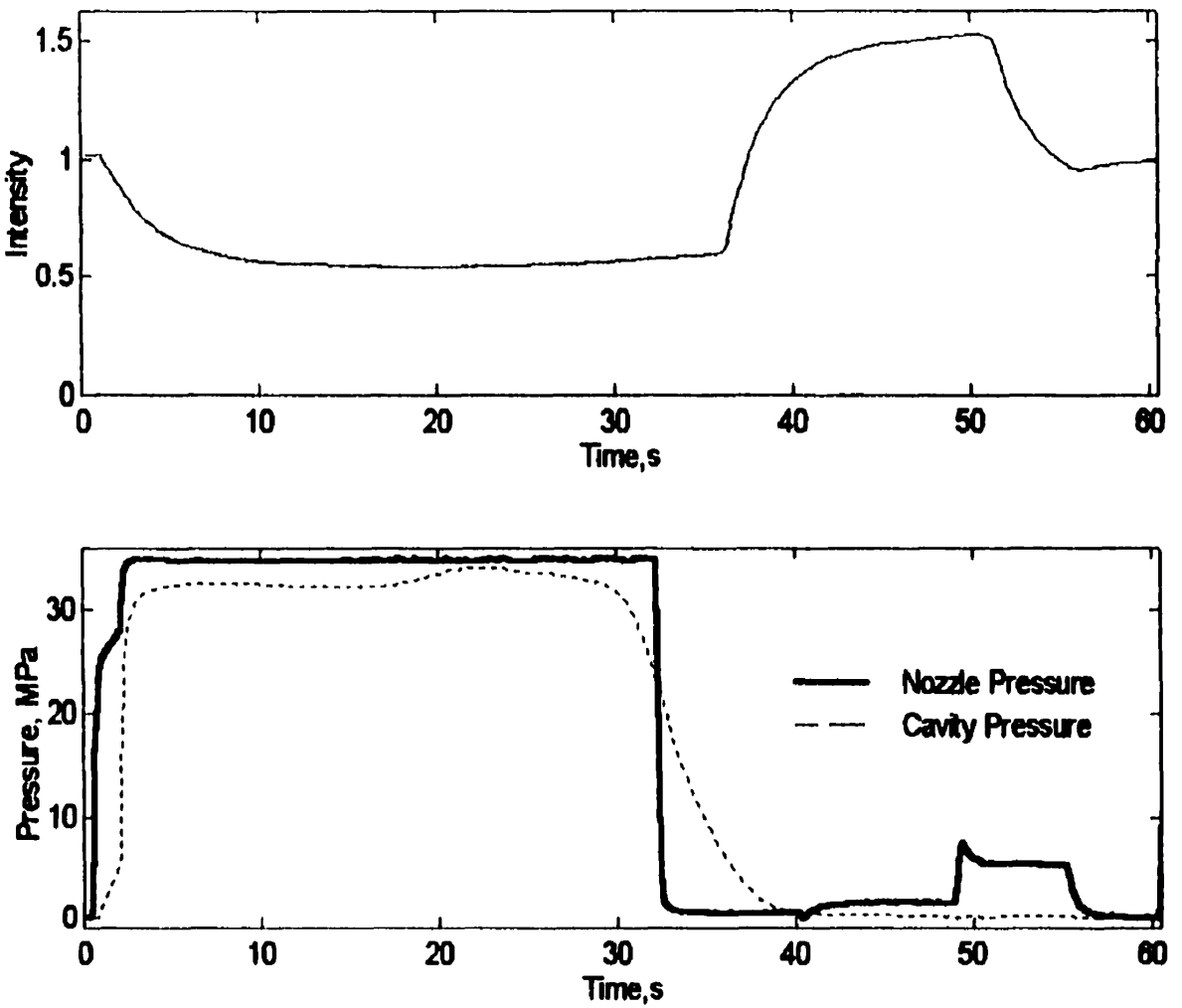

Figure 4.6B Plots of reflection intensity and pressure for HDPE, high cooling temperature experiment - HDPE/HT

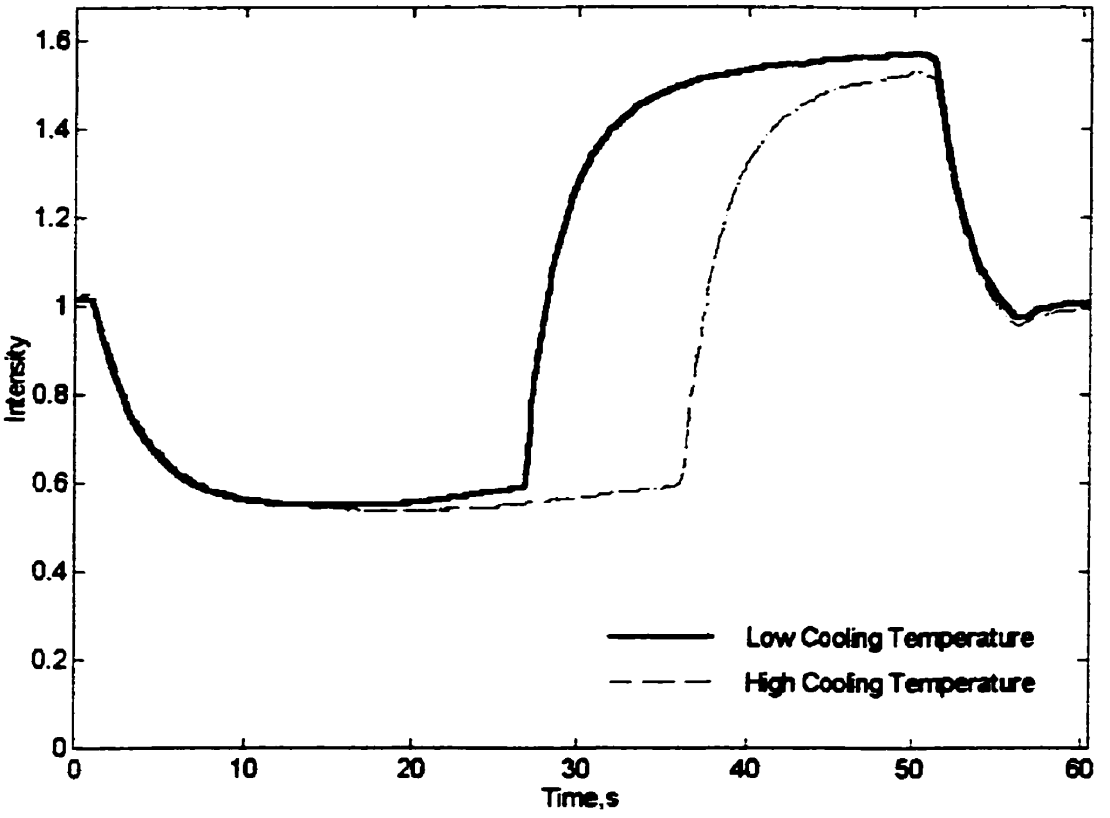

Figure. 4.6C: Comparison of intensities from the HDPE/LT and HDPE/HT experiments

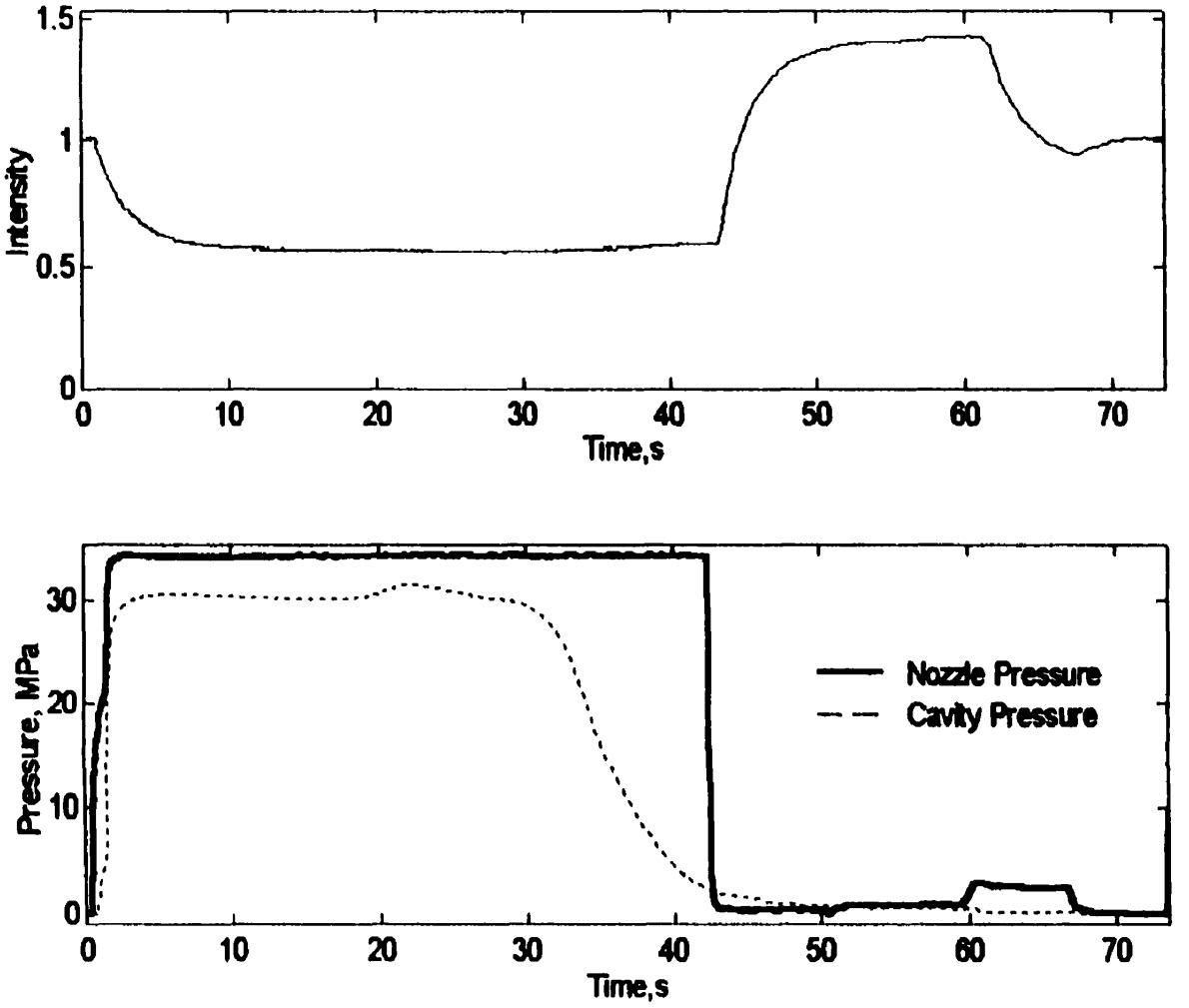

Figure 4.7A Plots of reflection intensity and pressure for polypropylene, low cooling temperature experiment - PP/LT

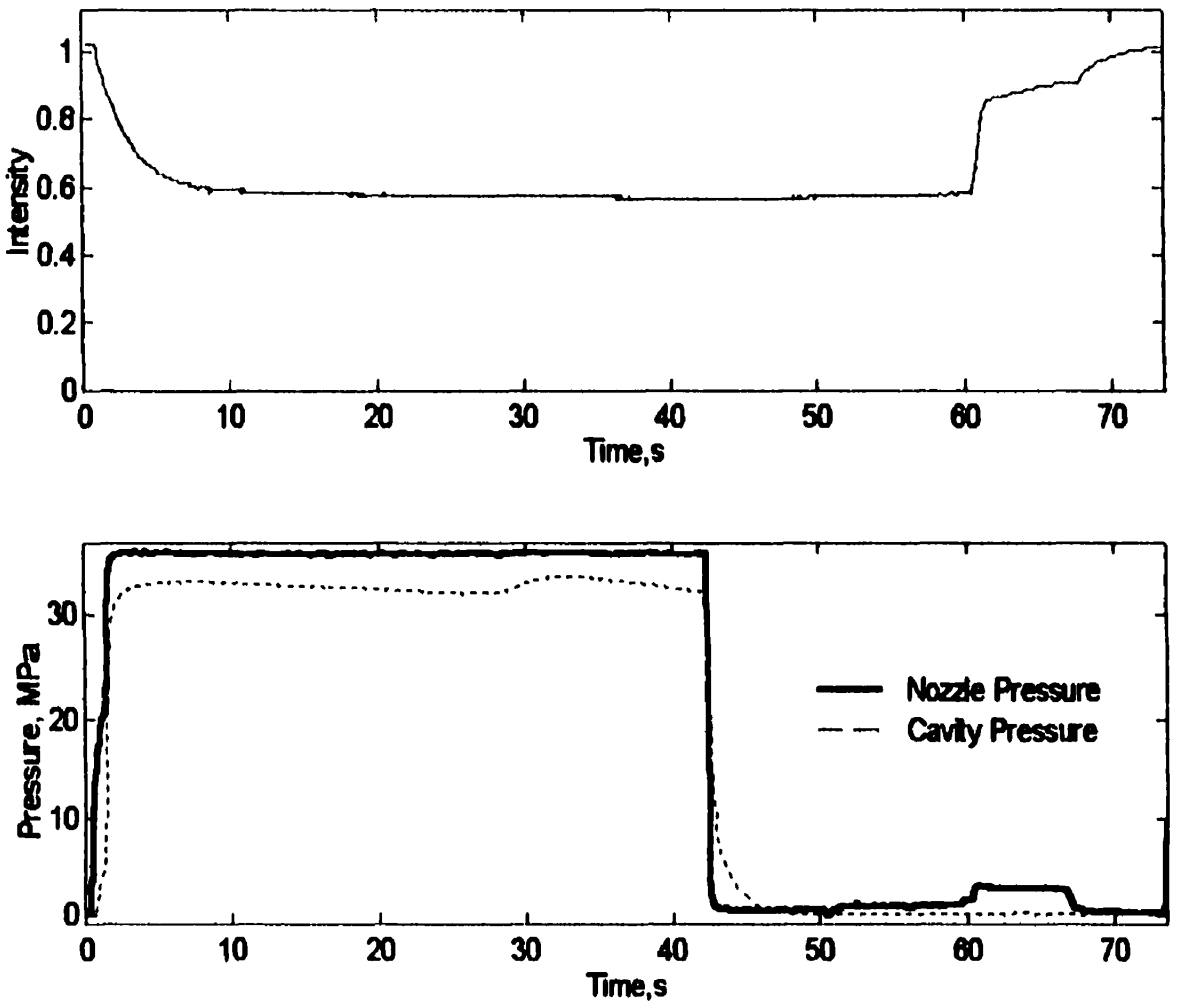

Figure 4.7B Plots of reflection intensity and pressure for polypropylene, high cooling temperature experiment - PP/HT

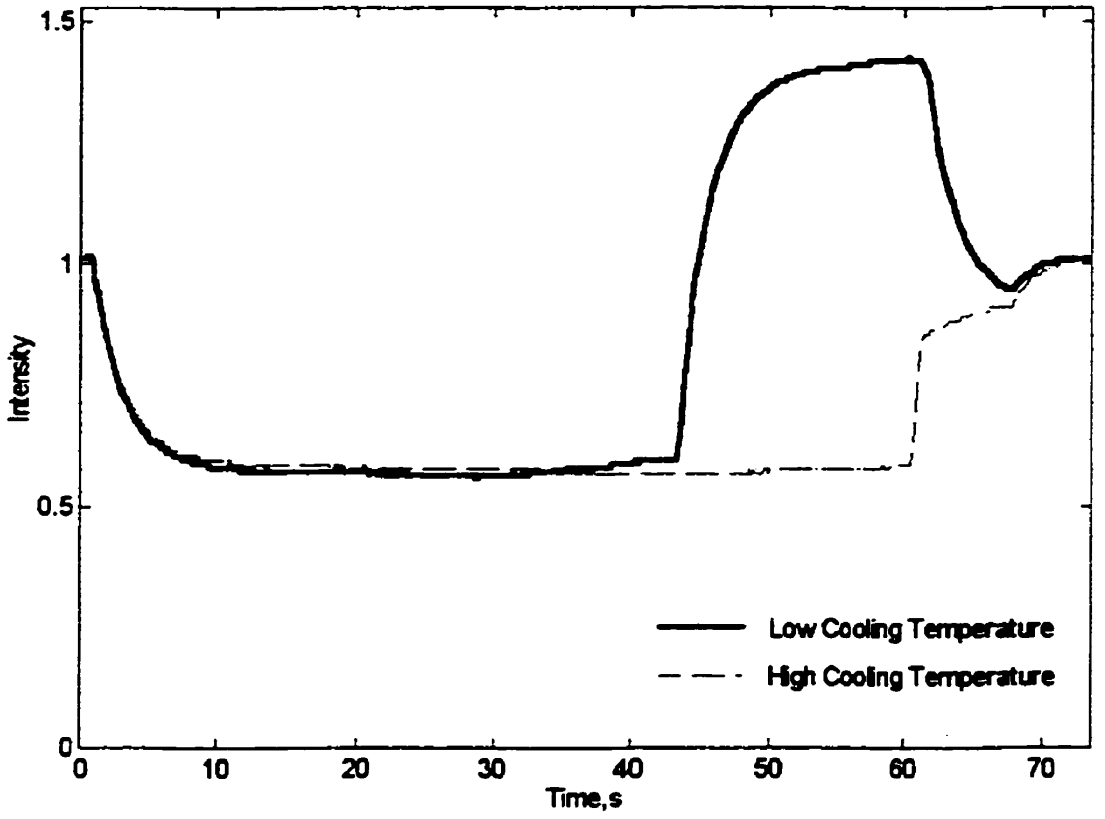

Figure 4.7C: Comparison of intensities from the PP/LT andPP/HT experiments

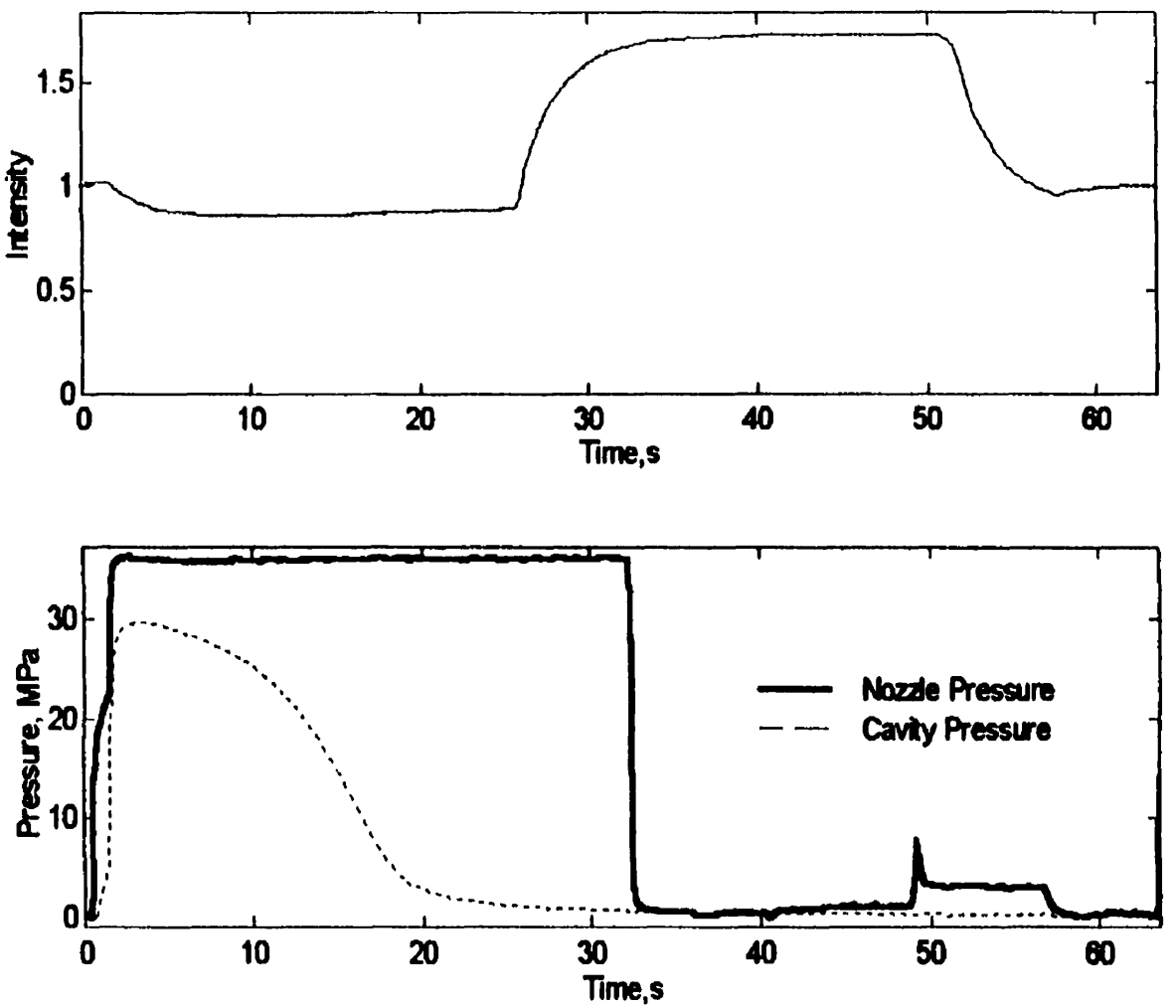

Figure 4.8A Plots of reflection intensity and pressure for polystyrene, low cooling temperature - PS/LT

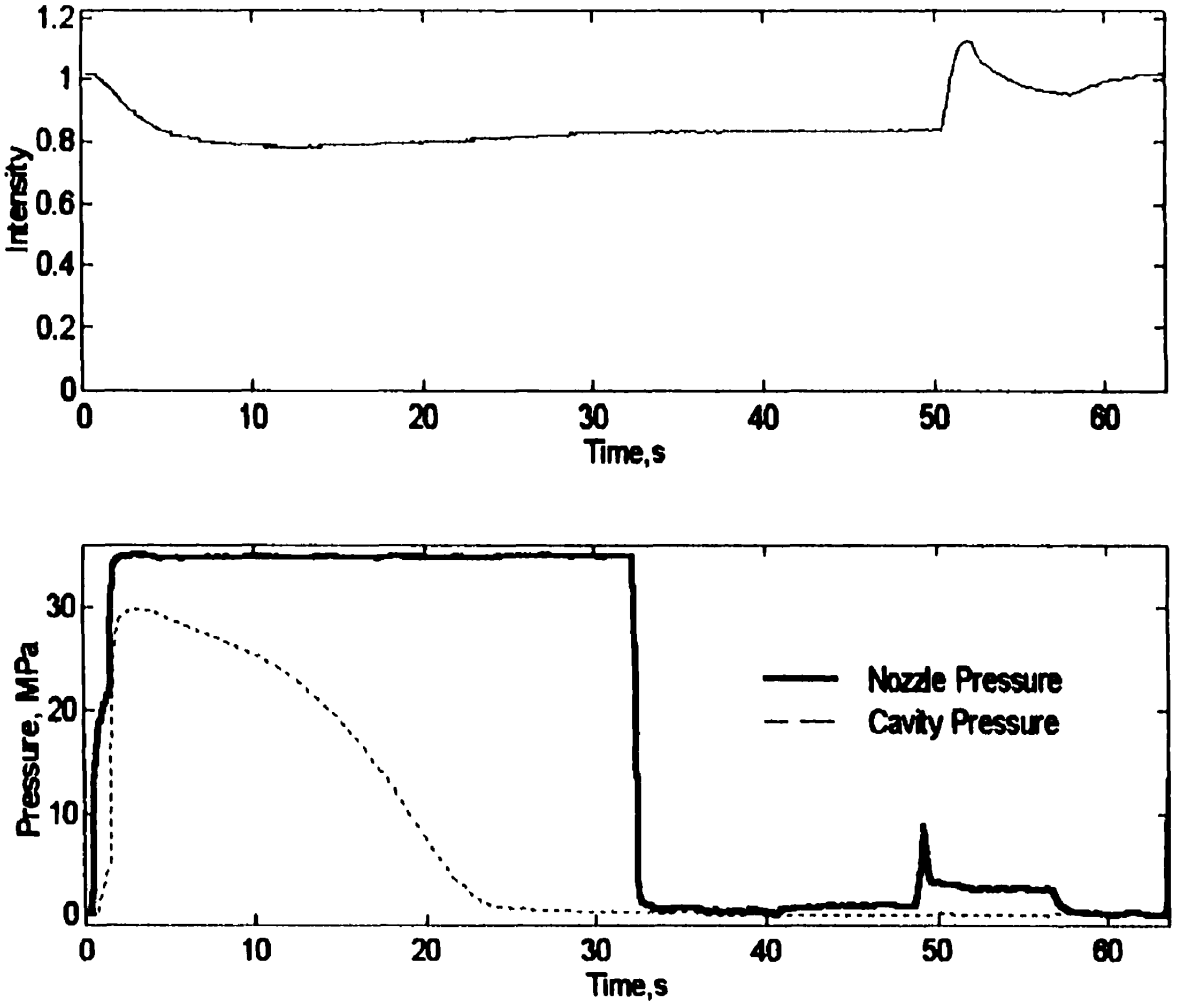

Figure 4.8B Plots of reflection intensity and pressure for polystyrene, high cooling temperature experiment - PS/HT

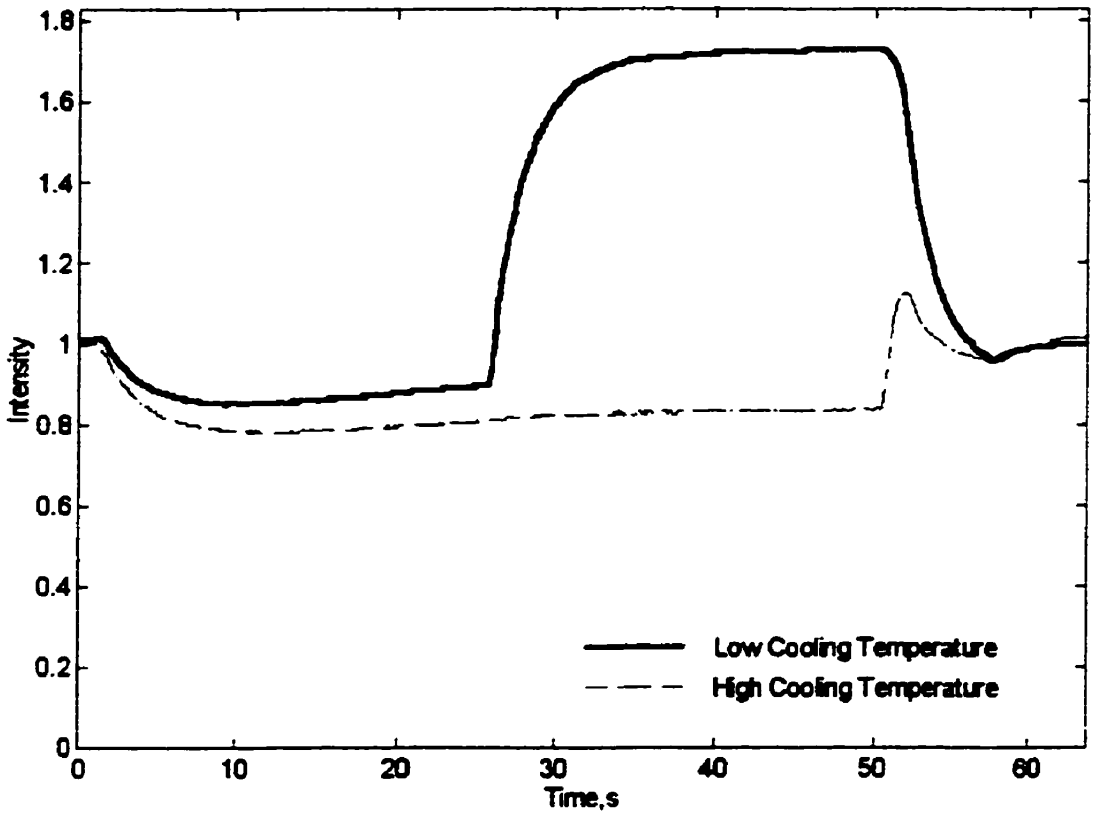

Figure 4.8C: Comparison of intensities from the PS/LT and PS/HT experiments.

4.6 Comparison to NIST Results

The results initially obtained in this work are compared to reports of the original experiments by Bur and Thomas [12]. Figure 4.9 shows their plots of reflection intensity data during the injection moulding cycle. According to our results presented in previous sections, their experiments were reproduced in the case of HDPE and PS. Their polypropylene results have a slightly different profile. The PP plots obtained from our work exhibit roughly the same pattern as our HDPE and PS plots. The difference between Bur and Thomas's PP curve and our PP results probably arise from different processing conditions that induce somewhat dissimilar crystallization. Different proportions of

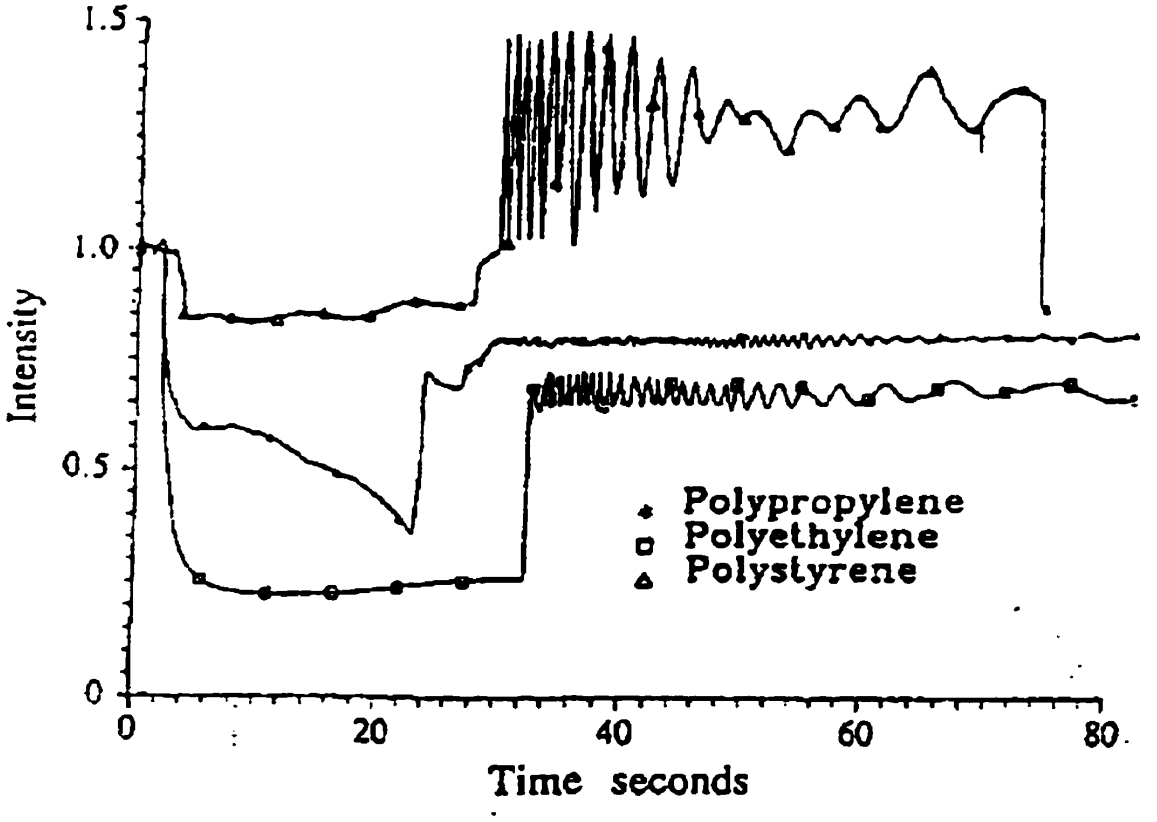

Figure 4.9 Reflection intensity curves obtained by Bur and Thomas [12].

amorphous and crystalline material in specimens are expected to produce different degrees of scattering. Both experiments were performed using polypropylene resins supplied by Himont, although it is not known if the same resin was used.

Bur and Thomas [13] developed a model that attempts to explain the most significant phenomena affecting light scattering in their injection moulding experiments. The model follows an approach by Yoon and Stein [10] for the scattering of polarized light by a crystallizing polymer melt. They claim very accurate reproduction of data, including a minimum of intensity values during the packing stage, which they attribute to a maximum reached in the scattering power of a crystallizing material. However, they do not use the model to explain the polyethylene data, which also should exhibit the reflection intensity minimum supposedly produced from crystallization effects. In fact, their polystyrene and

polyethylene curves are fairly similar, but it is unclear how their model can explain both of them. The polystyrene resin used by Bur and Thomas [12,13] is also an amorphous material.

Bur and Thomas [12,13] did not include the effect of pressure in their analysis. Our experiments included varied pressure conditions that allowed us to investigate other possibilities in the interpretation of intensity data. This is discussed in the following analysis of the light transmission phenomena through solidifying specimens.

4.7 Analysis of Experimental Results

The interpretation of data from the optical sensor requires consideration of other events that occur during the solidification of injection moulded specimens. In particular the shrinkage, orientation of polymer chains, and the relaxation of oriented polymer chains are phenomena known to affect the transmission of light.

4.7.1 Light Scattering by Injection Moulded Specimens

The crystallization process affects the scattering power of materials and is the main effect responsible for the differences between reflection intensities detected, as discussed in §4.4. Generally, the formation of randomly oriented crystals increases the scattering power and brings additional complexity to the interaction between the material and the light that traverses it.

In our experiments, the extent to which light is scattered by a crystallizing melt varies with time due to the changing proportions of crystalline and amorphous polymer present during the onset of crystallization. Yoon and Stein [10] reported that crystallizing polyethylene has a maximum scattering power when there are roughly the same volume fractions of amorphous and spherulitic polyethylene. Bur and Thomas [12,13] refer to this event to explain the minimum in their intensity curves. In our case, the presence of

crystals in an amorphous medium suggested that the analysis might be performed as a situation of light scattering by particles. The Mie Theory has been used to generate exact solutions to the problem of light scattering by a single particle [25], but during injection molding crystallization many particles with changing geometry are present. In addition, the influence of pressure and temperature makes the modeling of the interaction of light and material during crystallization of an injection moulded specimen a very complex problem. A solution using the Mie theory requires obtaining a phase function in terms of the geometry of the particle. Neither analytical nor numerical solution appears to have been attempted for the problem of melt solidification inside the mould cavity. A practical solution by means of numerical simulations requires a considerable experimental and analytical effort and is well beyond the scope of this work.

The main influences on transmission of light through solidifying amorphous materials such as polystyrene are refraction and reflection. In the case of our experiments, the incident beam reaches the interface between solid and melt polymer at an angle different of the normal to the interface. The beam is refracted at an angle that may be approximated using Snell's law [20]. In fact multiple refraction effects are taking place across the thickness of specimens in the cavity, as seen in Figure 4.11 (on page 68). The refraction angles change in time due to the change of shape of the melt core as it solidifies. An accurate quantification of these scattering effects requires a precise description of the evolution of the solidification process during the packing stage of injection moulding.

A model to evaluate the effects of changes in the value of refractive index of polystyrene during solidification of a specimen inside the mould is presented in §4.7.3. The effects of refraction are also considered. Geometric optics provides the basis to perform a qualitative analysis of refraction and reflection effects of the solidification process. No information was available concerning a detailed model for the evolution of the solidification process in terms of the shape and movement of the solid/melt interfaces.

One more influence on the scattering of light reaching the detector is the roughness of the opposite wall of the mould. Larena and Pinto [45] found that the surface roughness of thin

polyethylene films (30 μm, 50 μm and 70 μm) is a more important influence on the scattering of light than the degree of crystallinity of the samples tested. The incident light in these experiments had wavelengths between 210 and 290 nm. In our experiments the surface roughness is considered to be the main cause for the difference from the normalized 1 at the end of the packing stage in the polystyrene experiments. For polypropylene and HDPE the impact of the crystalline structures is considered the main factor, due to the relatively large thickness of the specimens.

4.7.2 Reflection Phenomena at the Interfaces

The shrinkage of specimens while they are still inside the mould strongly affects the total intensity signal measured. The jump in the intensity curve of Figure 4.1, at the time when the packing stage ends, is caused by the shrinkage of the specimen away from the mould wall. After this time, most of the light reflected back to the window comes from the specimen face that is just in front but separated from the window by a small air gap.

During the period of the packing phase before the separation of the specimen from the window, the reflection from the specimen walls is essentially constant. This follows from the fact that the refractive indices of the materials and the angles of incidence are not changing significantly at the interfaces between walls and specimen. However, from the moment when the gate cavity freezes, the specific volume decreases when the temperature falls, as no more melt enters the cavity. If the packing conditions are such that insufficient melt was injected into the cavity the volume of the part will be less than the volume of the cavity and the part surface will separate from the cavity walls. The separation gap must be on the order of several wavelengths: that is $2 - 3 \times 10^{-6}$ m. This is enough to cause significant reflection but not to affect part quality. For the rest of the cooling stage, the geometrical changes of the shrinking specimen are expected to increasingly affect the reflection at the far wall, as the angle of incidence gradually departs from the normal.

The internal interfaces between solid and liquid polymer also cause reflection and refraction. However, the angles at the interfaces are not precisely known. Furthermore, as solidification proceeds, the angles change according to the varying temperature (hence density) profile inside the cavity along its vertical axis [44]. Therefore, part of the incident light is reflected back to the window directly from the polymer interfaces, but a part of that reflected light is also scattered into the cavity. A quantification of this situation requires a detailed experimental analysis of the solidification profiles formed as the injection moulding cycle proceeds. Approximations to the effects of internal reflection are obtained in the next section.

4.7.3 *A Model of the Optical Sensor Reflected Light Intensity*

The model is aimed to simulate refraction and reflection effects that affect a laser beam transmitted across a polystyrene specimen that solidifies inside the mould cavity. The heat conduction equation for the solidification of melt, equation 4-1, was solved using a finite differences approach [46] and temperature profiles across the thickness of the specimen were generated. The liquid-solid interface was assumed to be where the temperature is equal to the shifted glass transition temperature, taking into account the effect of the cavity pressure.

Table 4.3a contains the group contribution of polystyrene to molar refraction R_{LL}, the molar mass of the polystyrene structural unit MM, and the glass transition point taken from [21]. The variation of thermal diffusivity with temperature was estimated by interpolating values from those available from Table 4.3b, taken from Dow Chemical Canada Inc. data sheets [43].

Table 4.5A Polystyrene molar refraction data

Property	Value
R_{LL}	33.679
MM, g/mol	104.1
Tg, °K	373

Table 4.5B Polystyrene thermal diffusivity

T, °K	Thermal Diffusivity × 10^{-8} m^2/s
100	24.52
200	16.42
300	12.35
400	8.28
500	8.02

The energy equation for heat conduction from the melt is presented as Equation 4-1. For amorphous polystyrene there is not a real phase change [8] so no latent heat term is included. Equation 4-1 is solved using a one dimensional finite-difference algorithm with a mesh size of 10, and time step of 0.05 seconds. A mesh size of 100 was also used and gave essentially the same results. A mesh size of 10 was preferred because of the shorter computation time.

$$\rho Cp \frac{\partial T}{\partial t} = k \frac{\partial}{\partial x}\left(\frac{\partial T}{\partial x}\right) \qquad 4\text{-}1$$

where ρ is the density,

Cp is the specific heat,

k is the thermal conductivity.

$$\tilde{p}\tilde{v}^5 = \tilde{T}^{3/2} - \ln \tilde{v} \qquad 4\text{-}2$$

Using the obtained temperature profile across the specimen thickness, the densities were calculated using the Hartmann-Haque equation of state [47].

where all the variables are so called reduced, as they are divided by reducing parameters according to [21]. p is pressure, T is temperature, and v is specific volume.

The refractive indices were calculated from their relationship to molar refraction and density, using the Lorentz and Lorenz expression [23], as mentioned in Chapter 2.

$$R_{LL} = \frac{n^2 - 1}{n^2 + 2}\frac{M}{\rho} \qquad \text{2-7}$$

where R_{LL} is the molar refraction,

M is the molar mass,

n is the refractive index.

The intensity of light transmitted across the specimen was calculated using Lambert's equation.

$$I = I_0 e^{\frac{-4\pi nKl}{\lambda}} \qquad \text{2-6}$$

where I, I_0 are final and initial light intensities,

K is the coefficient of extinction,

l is the distance traveled by the light,

λ is the wavelength of the incident light.

Snell's law determines the refraction effect at the interface between solid and liquid polymer.

$$n \sin i = n' \sin r \qquad \text{2-1}$$

where i is the angle of the incident beam,

r is the angle of the refracted beam.

The energy of the incident beam is divided into reflected and refracted portions. The intensity of the refracted beam is defined as the energy divided by the beam cross section area. The refracted beam cross section area may be calculated from the incident beam cross section area using the factor cos r/cos i [20].

Table 4.6. Parameter values used in the model execution

Parameter	Value
Mesh size	10
Time step, s	0.05
Time limit, s	10
Mould temperature, °C	25
Melt temperature, °C	260

The parameter that was varied in the model execution was the incident angle i from equation 2-1. Results from the model show that the variation of the refractive index does not cause a significant effect on the intensity of light transmitted across the specimen. However, the refraction effect becomes significant for angles larger than 30°. Figure 10 shows the intensity profile after 10 seconds of residence in the cavity. Data used for the simulation are presented in Table 4.4. The above period extends from the beginning of the packing stage to the freezing of polymer in the cavity gate.

The model results are compared to actual reflection intensity data for polystyrene in Figure 4.10. It may be appreciated that the initial period of the packing stage is similar to the profile obtained from the model execution for an angle of 30° at the first interface between solid and liquid polymer. It is unlikely that the angle between the interface and cavity wall is as large as 30°. However, there are several more interfaces in the path of the light before returning to the window. Then, it has been postulated that the propagation of

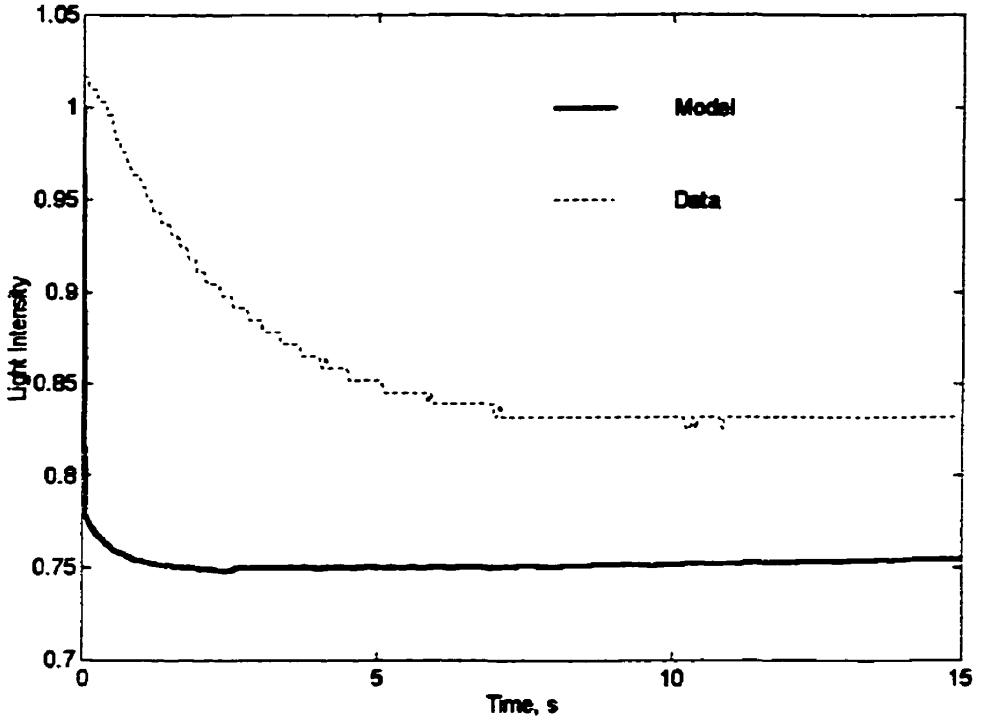

Figure 4.10 Calculated and measured reflection intensity. The incident angle for the model execution was 30°.

the angular refraction at every interface accounts for effects similar to a single, larger angle.

In Figure 4.10 the model curve does not include the initial time corresponding to filling of the mould cavity, so the data curve appears shifted to eliminate the filling period. Also, the lower intensity values are caused by the use of an inaccurate refractive index value for the steel of the mould. Nevertheless, the decreasing and stabilizing trend are similar.

In other executions of the model the incident beam angle was slightly varied on time, assuming that the interface angles are also varying as solidification proceeds. The curves obtained show the characteristic minimum in light intensity observed in the measured intensity curves. However, the initial intensity decrease could not be reproduced.

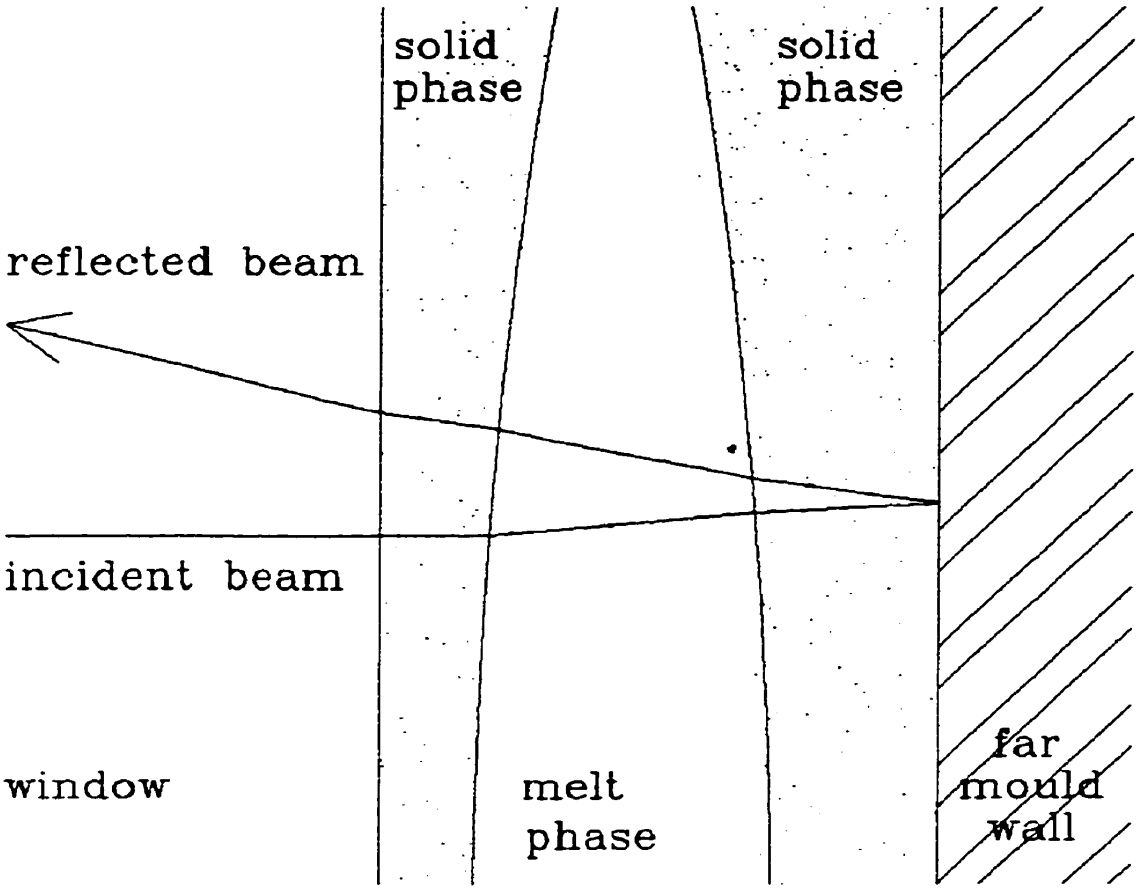

Figure 4.11 Approximation to the path of the laser beam inside the mould cavity during solidification

Figure 4.11 shows an approximation to the path of the light beam across the mould cavity during solidification. Apart from the initial interface between solid and liquid polymer, the beam must cross at least three more interfaces at angles different of the normal.

The surface roughness at the far mould wall contributes to scattering at larger angles, as mentioned in §4.7.1. Therefore, if the beam is deflected before reaching the wall, further reduction in the intensity is expected after reflection. This effect could not be included in the model due to the complexity of the effect of surface roughness on reflection.

The model does not accurately reproduce the optical phenomena of the experiments, because the evolution of the solidification process has not been studied in sufficient detail for the conditions used. The model attempts to account only for the most influential

effects: the refractive index change and refraction and reflection at the interfaces. The results obtained from the model are an approximation that is considered as an initial qualitative estimation of the actual phenomena involved.

When the cavity gate freezes, specimens solidifying inside the cavity show the effects of shrinkage. The sharp increase in reflection intensity at the end of the packing stage is associated with the separation of the polymer from the window, caused by shrinkage. From the reduction of the specimen thickness caused by shrinkage, an increase in the intensity of light transmitted across the specimen is expected, although the increase in the refractive index value upon complete solidification may actually compensate the change in total intensity [20]. More important is the disappearance of the solid-liquid interfaces when solidification is complete.

4.8 Convenience of the Optical Sensor for Monitoring Melt Solidification

The optical sensor has demonstrated that provides useful information about the rate of solidification of polymer melt inside the mould cavity. The interpretation and appropriate use of these data require the additional elements of pressure and temperature profile data.

Considering the results obtained, the sensor appears to be appropriate as a non-intrusive approach to identify solidification events during the packing stage of the injection moulding process. Since the solidification process may be controlled during this period, the sensor has relevance as a process control sensor.

A difficulty with the sensor arrangement is its dependence on the configuration and shape of the mould and light source which may further complicate its use. It has been shown that refraction is dependent on the shape of the interfaces between the solid and liquid masses of polymer inside the cavity and this strongly affects the measured intensity. This problem needs further work in simple cavities and those that have a more generalized form, which will lead to a more accurate model.

It is recognized that the effects on light transmission by crystallization of polymer melts are complex. The interaction between growing particles and light makes the interpretation a challenging problem. The analysis also requires consideration of orientation and relaxation effects on crystallization. Nevertheless, the general interpretation for the reflection intensity patterns described in §4.1 is valid for all materials used in this research. Information from a study of the morphology of injection moulded semi-crystalline specimens will aid the development of a model to explain the complex interaction of light and crystallizing specimens.

The optical sensor provides valuable information about the solidification rate. Additional studies of solidification dynamics are a natural complement to this work. The analysis of amorphous materials is the most convenient next step since this case is the simplest to interpret. The effect of pigmented and filled resins also needs to be studied if this technique is to be considered for practical applications.

Chapter 5

Conclusions

An optical sensor for monitoring the solidification of polymer melt inside the mould cavity of an injection moulding machine was constructed and tested.

The data produced by the sensor during the operation of the injection moulding machine allows the identification of the filling, packing, and cooling phases of injection moulding. The response of the sensor to different pressure levels was typical of a shifting of the polymer solidification. The sensor response to different cooling conditions also reflects the influence of different temperatures on the solidification rate. This sensitivity of the technique to pressure and temperature variations provides useful information for monitoring the solidification rate.

Reflection intensity profiles were obtained from the sensor during injection moulding of polyethylene, polypropylene, and polystyrene. The differences in material morphology cause distinct effects on the optical phenomena that are detected by the sensor. The differences in the refractive indices and light scattering properties were qualitatively as expected. Additionally, there is an indication that the geometry of the interface between solid and liquid phase significantly influence the reflection intensity values. Refraction at the interfaces was found to be responsible for the changing shape of the intensity curves during the packing phase of the injection moulding cycle.

The use of the sensor for control purposes requires further work to prepare a detailed model of the packing and cooling phases. The interaction between light and the solidifying melt inside the mould cavity is not completely understood in a quantitative sense. The initial effort to model the sensor reported in this work stresses the importance

of knowing more about the solid/melt interface geometry and the morphology of the solidifying polymer.

The study of semi-crystalline materials is particularly challenging because of the complex interaction between light and the crystalline structures forming and growing in the amorphous melt inside the mould cavity. Modeling the formation of the structures is a complex problem which is still under investigation at this time. Morphology analyses are more relevant in this case.

References

1. Rubin I.I., "Injection Molding Theory and Practice", *SPE Monographs v.1*, Wiley Interscience, New York, NY, USA (1972).

2. Woebken W., "International Plastics Handbook for the Technologist, Engineer and User /Saechtling", 3rd. ed., Hanser/Gardner, Munich, Germany (1995).

3. Gao F., Patterson W I., Kamal M R., "Cavity pressure dynamics and self-tuning control for filling and packing phases of thermoplastics injection molding", Polym. Eng. and Sci. v36 n9 pp1272-1285 (1996).

4. Varela A.E., Kamal M.R., Patterson W.I., "Method for estimating bulk melt temperature and part weight in injection molding of amorphous thermoplastics", Advances in Polymer Technology, v15 n1 pp17-28 (1996).

5. Rafizadeh M., Kamal M R., Patterson W I., "Physically-based adaptive control of cavity pressure in injection molding: Filling phase" Proc. SPE ANTEC, v1 pp582-587 Brookfield, CT, USA. (1997).

6. Tsoi Hoi-Pang, Gao Furong, "Fuzzy logic controller for injection ram velocity", Proc. SPE ANTEC, v1, pp641-644 Brookfield, CT, USA. (1998).

7. Franca D Ramos, Wen S-S.L., Jen C.K., Nguyen, K.T., Hebert H., "Advances in on-line monitoring of polymer injection molding process" Proc. IEEE Ultrasonics Symposium. v1 pp807-810, Piscataway, NJ, USA (1997).

8. Cowie J.M.G., "Polymers: Chemistry and Physics of Modern Materials", Blackie Academic and Professional, 2nd ed., Glasgow, UK (1991).

9. Thomas C.L., Tseng A.A., Bur A.J., Rose J.L., "Solidification Sensing for Closed Loop Control of Injection Molding Hold Time", Advances in Polymer Technology v15, n12 pp151-163 (1996).

10. Yoon D.Y. and Stein R.S., "Effects of Interference Between Anisotropic Scattering Entities on Light Scattering from Polymer Films. II. The Correlation Function Approach", *J. of Polym. Sci.: Part B: Polym. Phy.* 12, p735 (1974).

11. Bur A.J., Francis W.W., Thomas C.L., Rose J.L, "In-Line Optical Monitoring of Polymer Injection Molding", *Polym. Eng. and Sci.*, 34, n8, pp671-679 (1994).

12. Bur A.J, Thomas C.L., "A Multi-Functional Optical Sensor for Monitoring Polymer Injection Molding", *Proc. SPE ANTEC pp*2798-2804 (1995).

13. Bur A.J., Thomas C.L., "Optical Monitoring of Polypropylene Injection Molding", *Proc. SPE ANTEC pp*415-420 (1997).

14. Swanson E.A., "High Resolution Imaging of Polymer Structure Using Optical Coherence Tomography", *Proc. SPE ANTEC* pp2794-2797 (1995).

15. Li S., Migler K.B., Hobbie E.K., Kramer H., Han C.C., Amis E.J., "Ligh-Scattering Photometer with Optical Microscope for the In-Line Study of Polymer Extrusion", *Journal of Polymer Science: Part B: Polymer Physics*, 35, pp2935-2943 (1997).

16. Gendron R., Tatibouët J., Guèvremont M., Dumoulin M., Piché L., "Ultrasonic Behaviour of Polymer Blends", *Polym. Eng. and Sci.*, 35, pp79-91 (1995).

17. Verdier C., Piau M., "Analysis of the Morphology of Polymer Blends Using Ultrasound", *J. Phys. D: Appl. Phys.*, 29, pp1454-1461 (1996).

18. Piché L., Lévesque D., Gendron R., Tatibouët J., "Ultrasonic Probe of Polymer Flows", *Proc. SPE ANTEC* pp2715-2719 (1995).

19. Thomas C.L., Adebo A.O., Bur A.J., "Ultrasonic measurement of Polymer Material properties during Injection Molding", *Proc. SPE ANTEC* pp2236-2239 (1994).

20. Longhurst R.S., "Geometrical and Physical Optics", second edition, Longmans, London, UK (1967).

21. Van Krevelen, D.W., "Properties of Polymers: their Correlation with Chemical Structure, their Numerical Estimation and Prediction from Additive Group Contributions", Elsevier: Amsterdam, New York (1990).

22. Gladstone J.H. and Dale T.P., Trans. Roy. Soc. A 148, 887, London UK (1858), cited in reference [21].

23. Lorentz H.A., Wied. Ann. Phys. 9, 641 (1880), cited in reference [21]..

24. Goedhart D.J., Communication Gel Permeation Chromatography International Seminar, Monaco, Oct. 12-15, (1969), cited in reference [21].

25. Belanger C., "Characterization of Polymer Blend Morphology from Patterns of Reflected Scattered Light", Ph.D. Thesis, McGill University, Montreal (1992).

26. Danson Corporation, "Danson Metalmec 60 SR Instruction Book", Scarborough, Ontario, Canada (1969).

27. Gao F., "The Control of Cavity Pressure throughout the Injection Moulding Cycle", Ph.D. Thesis, McGill University, Montreal (1993).

28. Abu Fara D., "Control of Nozzle and Cavity Pressure during Filling and Packing in Thermoplastic Injection Molding", Ph.D. Thesis, McGill University, Montreal (1988).

29. Analog Devices, "RTI-220/222 User's Manual", Norwood, Ma., USA (1989).

30. Analog Devices, "RTI-217 User's Manual", Norwood, Ma., USA (1989).

31. Fusser H.B., "A Man-Machine Interface for PC-Controlled Injection Molding", M.Eng. Thesis, McGill University, Montreal (1991).

32. McDowell S.G., "Watcom C Language Reference", Watcom Publications Ltd., Waterloo, ON, Canada (1987).

33. Didsbury K., Leroux P.N., and Ostrander J.M., "QNX 4.1 Operating System User's Guide", Quantum Software Systems Ltd., Kanata, Canada (1992).

34. The Optikon Corporation Ltd., "He-Ne Laser System Instruction Manual (1-5 milliwatt systems)", Waterloo, Ontario, Canada (1985).

35. Edmund Scientific, "Optics and Optical Instruments Catalog", Barrington, New Jersey, USA (1997).

36. CVI Laser Corp."Optics and Coatings Catalog", Putnam, Connecticut, USA (1997).

37. Oriel Instruments, "Photomultiplier Detection System Model 7070 Instruction Manual", Stratford, Connecticut, USA (1991).

38. Oriel Corporation, "Optics and Filters", Oriel Catalog vol. III, Stratford, Connecticut, USA (1990).

39. Summers Optical Catalog III, Fort Washington, Pennsylvania, USA (1997).

40. Nova Chemicals Ltd., Sclair Polyethylene 2908 Product Data Sheet, Calgary, Alberta, Canada (1998).

41. Kamal M.R., Personal communication, 1998.

42. Montell Polyolefins, Pro-Fax 6523 Data Sheet, Montell North America Inc., Wilmington, De, USA (1997).

43. Dow Chemical Canada Inc., Styron 685D Polystyrene Resins Product Data Sheet, Sarnia, Ontario, Canada (1992).

44. Manero F., "Cavity Temperature Measurement and Control in Thermoplastics Injection Moulding", M.Eng. Thesis, McGill University, Montreal (1996).

45. Larena A. and Pinto G., "The effect of surface roughness and crystallinity on the light scattering of polyethylene tubular blown films", Polym. Eng. And Sci. v.33, pp742-747 (1993).

46. Erhun M., Advani S., "A Predictive Model for Heat Flow during Crystallization of Semi-Crystalline Polymers", *Journal of Thermoplastic Composite Materials* 3, 90-109 (1990).

47. Hartmann B., and Haque M.A., J. Appl. Polym. Sci. 30, 1553 (1985).

48. Ozisik M.N., "Heat Conduction", John Wiley and Sons, New York (1979).

49. Kamal M.R., Mutel T., Salloum G., Garcia-Rejon A., "Heat Transfer Measurement at the Mold Surface during Injection Molding of Thermoplastic Melts", SPE ANTEC, 35, 483 (1991).

50. Ruscitti G., "The Measurement and Control of Nozzle Melt Temperature in Injection Moulding", M.Eng. Thesis, McGill University, Montreal (1992).

51. Varela A., "Estimation and Control of Part Weight and Relevant Process Parameters in Injection Molding of Amorphous Thermoplastics", Ph.D. Thesis, McGill University, Montreal (1996).

52. Rafizadeh M., "Physically-Based Dynamic Model for the Control of Cavity Pressure in Thermoplastics Injection Molding", Ph.D. Thesis, McGill University, Montreal (1997).

Appendix A

Injection Moulding Machine Settings

The IMM settings used for the experiments are presented in Tables A.1 and A.2. An injection moulding cycle was divided into four periods, as proposed in [6]. The initial stage, called "injection", covers the time while the screw is being pushed forward, applying pressure into the mould cavity. When the pressure is released from the screw, it moves back slightly, but is not yet fully retracted. This is called the "holding" period. Next the screw moves back and rotates to generate melt for the next cycle while the specimen continues cooling in the mould. This is the "cooling" period. Finally, the "recycling" period extends from the moment when the specimen is ejected, until the time when the screw moves forward again to inject melt for the next specimen. The mould is opened, the part ejected and the mould is then closed during this period.

Table A.1 Settings for the IMM data acquisition boards

Period	Setup Timers			Sampling rates	
	PE	PP	PS	Fast ADC	Slow ADC
Injection	32	40	32	50	1000
Holding	8	8	8	100	1000
Cooling	10	10	10	200	1000
Recycling	10	13	13	250	1000

Table A.2 Barrel temperatures used

Material	Temperature, °C			
	Zone 1	Zone 2	Zone 3	Zone 4
Polyethylene	210	190	170	150
Polypropylene	250	225	200	175
Polystyrene	260	230	200	170